PREDICTIVE MODELING OF IN SITU RETARDATION OF REACTIVE TRACERS DURING C-WELL TESTING AT YUCCA MOUNTAIN, NEVADA

By

Bruce A. Robinson

Abstract

Preliminary modeling has been performed in the C-wells reactive tracer project at Yucca Mountain, Nevada, in three areas: tracer experiment design, modeling to provide information for laboratory studies, and model development. Interwell experiments appear to be more appropriate than do drift pumpback experiments, and these should be run without recirculating the tracer. Parameter sensitivity calculations were used to identify appropriate sorption parameters and to examine variables that must be considered in laboratory experiments. Models based on residence time distribution theory have been developed as an alternative modeling approach for reactive tracer experiments. In addition, more traditional finite difference and finite element codes will be used. Finally, a new fracture network model is being developed to simulate flow and transport between wellbores in fractured media.

Chapter 1. Introduction

The C-wells conservative and sorbing tracer experiments are designed to examine the transport and sorption properties at one location in the saturated zone beneath Yucca Mountain. The C-wells are three wellbores drilled into the saturated zone and are devoted to hydrology and transport studies. The primary goals of the reactive tracer experiments at the C-wells are

1) to examine the transport characteristics of conservative and sorbing solutes in the saturated zone;
2) to assess the role of fractures in solute transport in the saturated zone;
3) to evaluate the usefulness of inert and sorbing tracer laboratory and field experiments for determining transport characteristics;
4) to develop a modeling approach for interpreting single-well and multiwell sorbing tracer field experiments; and
5) to use the results to plan reactive tracer field experiments elsewhere in the saturated zone at Yucca Mountain.

The US Geological Survey (USGS) and Los Alamos have proposed a comprehensive series of hydraulic, conservative tracer, and reactive tracer experiments at the C-wells. In the first part of the investigation, the USGS will perform hydraulic experiments in single wells and interference experiments between wells. Using packers in each well, they will identify zones of flow communication between wells at different depths and thus hopefully characterize the three-dimensional hydraulic conductivity tensor at the site.

Next, the USGS will carry out conservative tracer experiments to supplement their hydrology results. Three tracer techniques have been proposed: (1) the interwell recirculating experiment, with injection into one well and pumping at the same rate from another; (2) the convergent tracer experiment, in which tracer is deposited downhole in a stagnant well while pumping from a second well; and (3) the single-well

drift-pumpback experiment, in which tracer is deposited downhole, allowed to drift with the prevailing groundwater flow field, and then is pumped back up the same well. This series of experiments should characterize the hydrology and transport properties at the C-wells, allowing extrapolation to a larger regional scale in the saturated zone.

Los Alamos's proposed experiments at the C-wells are designed to examine the sorption characteristics of the site, a property not addressed in the USGS's experiments. The experimental approach is similar to the USGS's. First, using complex flow and transport models, we will attempt to understand the physics of the hydrology, conservative tracer, and reactive tracer behavior of the site. Then, inferences will be drawn about the overall performance of the saturated zone as a barrier to radionuclide transport.

Thus, the proposed experiments focus on the fundamentals of reactive solute transport in fractured porous media as well as provide information on the transport properties of the saturated zone beneath Yucca Mountain. The project consists of three phases: (1) a preliminary modeling and laboratory experimental stage to design the field experiments and identify appropriate reactive tracers; (2) the field experiment phase; and (3) the postexperiment modeling to interpret the data and draw conclusions addressing the experiment goals listed above.

This report summarizes preliminary modeling and code development work performed to date. The preliminary modeling serves two purposes. First, modeling allows us to determine the likely behavior of the experiments under different flow scenarios, both to define appropriate sorption parameters and characteristics for field experiments as well as to identify the most appropriate mode of operation. Second, modeling calculations can be used to design a laboratory experimental program to examine potential reactive tracers. Chapters 2, 3, and 4 report these modeling results. The code development section of this report (Chapter 5) summarizes our proposed modeling approach, describes codes currently available, and reviews work performed so far to develop new models for interpreting the field results.

This work is supported by the Nevada Nuclear Waste Storage Investigations Project which is managed by the Waste management Project Office of the US Department of Energy.

Chapter 2. Equilibrium Adsorption Modeling

2.1 Introduction

Reacting or sorbing solutes have the potential to provide information not readily available from conventional hydrologic and inert tracer field experiments. In this chapter, we develop and use a one-dimensional model of dispersion and sorption in a porous medium to illustrate the behavior of inert and sorbing tracers in field studies and identify appropriate ranges of values for tracer sorption parameters and field experiment operating conditions. In addition, the sorption model formulated here can be used in future laboratory column studies. When the batch reactor equilibrium sorption parameters are known, the code can be used to plan flowing column sorption experiments and to model the results obtained.

Specifically, two major sets of parameters are addressed in this modeling study: the sorption characteristics of the tracer and the operating configuration and conditions of the field experiment. The tracer sorption reaction with the rock may be either strong or weak, and it may reach equilibrium very quickly or be controlled by the reaction kinetics. An equilibrium adsorption model is used to examine the effect of the strength of the sorption reaction for different operating conditions to identify the optimum range of parameter values. The effect of the nature of the equilibrium adsorption isotherm (linear versus nonlinear) will also be investigated.

The choice of operating configuration and conditions of the tracer experiments are also addressed in this chapter. Three types of inert tracer experiments have been proposed by the USGS to investigate the hydrologic properties at the C-wells: interwell recirculating, interwell convergent, and single-well drift pumpback experiments. There are significant advantages to carrying out sorbing tracer experiments in these modes of operation at similar conditions and with the same downhole hardware that was used in the conservative tracer experiments.

First, interpretation of a sorbing tracer field experiment will require a comparison with an inert tracer response. This is most effectively accomplished by performing the experiments simultaneously. Furthermore, changes in downhole configuration such as location of packers require expensive rig operations that, if possible, should be avoided.

However, these considerations should not completely dictate the design of sorbing tracer experiments. If experiments that are appropriate for conservative tracers do not provide useful results with sorbing tracers, they should not be run. This chapter also addresses this question for interwell and single-well experiments.

2.2 Model Development

To perform preliminary scoping calculations to address the issues discussed above, the one-dimensional, transient, axial dispersion equation will be employed. For inert, nonsorbing chemical species,

$$\frac{\partial C^*}{\partial t^*} = D_e \frac{\partial^2 C^*}{\partial x^{*2}} - U \frac{\partial C^*}{\partial x^*} \quad , \tag{1}$$

where C^* is the concentration, t^* is time, and x^* is distance in the direction of flow. The model assumes one-dimensional fluid flow in the x-direction at velocity U, with an effective axial dispersion coefficient D_e. This effective dispersivity is not merely the molecular diffusion coefficient, but rather accounts for tracer spreading caused by fluid flow paths of different size, length, and hydraulic conductivity. Obviously, this model is more simplified than the more realistic modeling geometries that can be handled by complex finite difference or finite element transport codes. Nonetheless, it is useful for these scoping calculations because the effect of various operating parameters, tracer adsorption characteristics, and modes of tracer injection and measurement can be examined quickly, easily, and in sufficient detail to address the issues cited above.

Adsorption is modeled by incorporating the additional term $a^*\partial S^*/\partial t^*$ in the mass balance equation to account for the tracer residing on the rock surface. Equation (1) then becomes

$$\frac{\partial C^*}{\partial t^*} + a^* \frac{\partial S^*}{\partial t^*} = D_e \frac{\partial^2 C^*}{\partial x^{*2}} - U \frac{\partial C^*}{\partial x^*} \quad . \tag{2}$$

The term $a^*\partial S^*/\partial t^*$ represents solute storage in terms of a surface concentration S^* (mass of tracer per unit surface area) and a^*, the rock surface area to fluid volume ratio. This formulation is used because flow in the C-wells experiments is expected to be dominated by fracture flow. Solute sorption on a fracture will thus depend on the fracture surface area rather than on the mass of rock contacted, as in the usual sorption formulation using K_d.

The term $a^*\partial S^*/\partial t^*$ must be represented by using a model for the rock-solute interaction. Typically, either a kinetic rate law or equilibrium adsorption is assumed. Kinetic modeling requires an additional differential equation to represent the rates of adsoption and desorption from the rock surface. Sorption kinetics are treated separately in Chapter 3. A simpler approach is to assume that compared with the overall transit time of the solute, the time constant for the reaction is very small, so that the solute is in chemical equilibrium with the rock at every position. If this is true, an equilibrium relation between C^* and S^* can be used to eliminate S^* from Eq. (2). In the present study the reversible Langmuir adsorption isotherm is assumed:

$$S^* = \frac{b_1 C^*}{1+b_2 C^*} \quad , \tag{3}$$

where b_1 and b_2 are derived from experimentally determined parameters for the adsorption and desorption reactions. Figure 1 shows a typical adsorption isotherm for a reaction with a Langmuir equilibrium sorption isotherm. At low concentrations, corresponding to low surface coverage of the solute on the rock surface, the isotherm is linear. At high concentrations, where the available surface sites are filled, an increase in solute concentration in the fluid results in no further sorption onto the rock. This two-parameter model is flexible enough to

span a large range in possible types of solute behavior. Two classes of equilibrium sorption reactions will be examined in the present study: a linear adsorption isotherm with $b_2 = 0$ and nonlinear adsorption with nonzero values for b_1 and b_2.

To incorporate the Langmuir adsorption isotherm into the mass balance equation, the derivative $\partial S^*/\partial t^*$ is calculated from Eq. (3):

$$\frac{\partial S^*}{\partial t^*} = \frac{\partial S^*}{\partial C^*}\frac{\partial C^*}{\partial t^*} = \frac{b_1}{(1+b_2C^*)^2}\frac{\partial C^*}{\partial t^*} \quad . \tag{4}$$

Substituting this expression into Eq. (2) and nondimensionalizing,

$$\left[1+\frac{a_L}{(1+bC)^2}\right]\frac{\partial C}{\partial t} = Pe^{-1}\frac{\partial^2 C}{\partial x^2} - \frac{\partial C}{\partial x} \quad , \tag{5}$$

where $C = C^*/C_{ref}$, $x = x^*/L$, $Pe = UL/De$, $t = Ut^*/L$, $a_L = b_1a^*$, and $b = C_{ref}\,b_2$. This expression is the dimensionless mass balance equation for a solute undergoing dispersion and an equilibrium, reversible adsorption reaction in a one-dimensional flow field. The only difference from the more familiar nonsorbing convective-dispersion equation is the multiplier of the time derivative of concentration; the equation reduces to the nonsorbing tracer mass balance when $a = 0$. When adsorption is important, this multiplier is a constant, a_L, for linear adsorption and a concentration-dependent term for nonlinear adsorption.

The appropriate boundary conditions at the two ends of the flow system are the flux-based boundary conditions proposed by Danckwerts (1958):

$$x = 0: \quad C - Pe^{-1}\frac{\partial C}{\partial x} = C_{in} \tag{6}$$

$$x = 1: \quad \frac{\partial C}{\partial x} = 0 \quad , \tag{7}$$

where C_{in} is the dimensionless inlet concentration. These boundary conditions are valid for one-dimensional flow with closed boundaries, inlet and outlet ports with negligible axial mixing compared with that inside the system. The inlet condition sets the mass flow rate of tracer into the system equal to the mass flux inside the system at x =

0. The outlet condition is obtained from similar mass balance considerations. At large Peclet numbers (little dispersion), the solution with these boundary conditions is nearly identical to the more familiar error function solutions obtained when the boundary conditions are assumed to be

$$\frac{\partial C}{\partial x} = 0 \ , \ x = \pm \infty \quad . \tag{8}$$

However, for larger levels of dispersion (smaller Pe), Eq. (8) is no longer valid, and the Danckwerts boundary conditions must be employed. The resulting differential equation and boundary conditions are most easily solved numerically, as general analytical expressions do not exist for Eq. (5) with the flux-based boundary conditions. The computer code SORPTION was written to solve the equations by finite difference techniques.

2.3 Numerical Solution Procedures

To solve Eq. (5) and the boundary conditions of Eqs. (6) and (7), conventional finite difference techniques have been employed. The spatial derivatives $\partial C/\partial x$ and $\partial^2 C/\partial x^2$ are calculated by using a centered difference approximation. The finite difference grid consists of M equally spaced nodes, and the centered difference equation is written for each of the interior nodes (2 through M-1):

$$\frac{\partial C_i}{\partial t} = \frac{\frac{1}{h^2 Pe}\left(C_{i+1} - 2C_i + C_{i-1}\right) - \frac{C_{i+1} - C_{i-1}}{2h}}{\left(1 + \frac{a_L}{(1+bC_i)^2}\right)} \ , \tag{9}$$

where h is the nondimensional spacing between the nodes, equal to 1/(M-1). To incorporate the boundary conditions, a commonly used procedure outlined by Finlayson (1980) is employed. The centered difference equation [Eq. (9)] is written for the inlet and outlet nodes (1 and M, respectively), which creates fictitious concentrations C_0 and C_{M+1} outside the mesh. However, if centered difference approximations

are also written for the boundary conditions, expressions for C_0 and C_{M+1} are derived and used to eliminate these imaginary concentrations. The resulting equations for the two boundaries are

$$\frac{\partial C_1}{\partial t} = \frac{(1+bC_1)^2}{a_L+(1+bC_1)^2}\left[\frac{1}{h^2Pe}(2C_2 - 2C_1 + 2hPe(C_{in}-C_1)) - Pe(C_1-C_{in})\right] \tag{10}$$

$$\frac{\partial C_M}{\partial t} = \frac{(1+bC_M)^2}{a_L+(1+bC_M)^2}\left[\frac{2}{h^2Pe}(C_{M-1} - C_M)\right] \quad . \tag{11}$$

The time integration is solved by the Crank-Nicholson method, which allows a degree of flexibility between a fully implicit and fully explicit formulation. For Eqs. (9), (10), and (11), the approximation is

$$\frac{C(t+\Delta t) - C(t)}{\Delta t} = (1-\beta)f[C(t)] + \beta f[C(t+\Delta t)] \quad , \tag{12}$$

where $f[C(t)]$ is the right-hand side of the equation evaluated at time t, and β is a parameter between 0 and 1 used to set the degree of implicitness of the solution. For example, $\beta = 0$ is the explicit Euler's method, $\beta = 1$ is the implicit Euler's method, and $\beta = 0.5$ is trapezoidal integration.

When Eq. (12) is written for each nodal equation, the result is a system of M nonlinear equations with M unknowns (the C_i's). The solution procedure used for solving these equations allows either a full or quasi-Newton method. First, the equation set is rewritten in residual form ($R_i = 0$) by grouping the entire expression on one side of the equation. At each time step, the full Newton's method requires the following matrix equation to be solved iteratively until all R_i are close to 0:

$$\underline{\underline{J}}^j \, \underline{\delta}^{j+1} = \underline{R}^j \quad , \tag{13}$$

where j is the number of the iteration, the elements of the vector $\underline{\delta}^{j+1}$ are given by $C^j - C^{j+1}$, and the elements of the tridiagonal Jacobian matrix $\underline{\underline{J}}$ are given by $\partial R_i / \partial C_k$. The values of J_{ik} are calculated from analytic expressions derived from the residual equations. In general

the nonlinear equations result in concentration-dependent expressions for the J_{ik}, which must be recalculated at each iteration in the full Newton method. Since this can sometimes result in large calculation time per iteration without a significant improvement in the rate of convergence, the code was written with the provision of employing the quasi-Newton method, in which the J_{ik} are calculated only at the beginning of each time step by using the concentrations at the previous time step. These same concentrations also serve as the first guess in the iterative solution of the equation set. When the change in each concentration from one iteration to the next is less than a user-selected convergence criterion, convergence is assumed and a new time step is taken. This convergence criterion is typically set at least 4 orders of magnitude below the inlet concentration to assure accuracy of the solution.

2.4 Simulation Capabilities of the Model

The nature of the equilibrium adsorption isotherm can be varied by setting the values of the two parameters in the Langmuir model. In addition, the model is capable of simulating solute transport for different concentration inputs and modes of operation of the system.

The model can simulate either a step change in solute concentration or the injection of a pulse of tracer at a given concentration for a given duration. For pulse injection, the user supplies two times t_1 and t_2 and three inlet concentrations. The first concentration is the value from time 0 to t_1, the second is the value between t_1 and t_2, and the third is the inlet concentration after t_2. This provision allows a pulse of solute to be injected either initially or after a specified period of time. To model a step response, the three concentrations are set to the same value.

Two modes of operation of the sorbing tracer experiment can be simulated with the model: the flow-through and injection-backflow (or drift-pumpback) modes. Thus the model is capable of simulating both interwell and drift-pumpback tests but cannot be used to evaluate

differences between the recirculating and convergent interwell tests, which differ mainly in the type of flow patterns established between the wells.

An interwell tracer experiment is simulated by plotting the concentration-time behavior at node M, the concentration at the outlet of the flow system. Simulation of the injection-backflow operation requires modeling the two phases of the experiment. During injection, the code is operated in the forward direction as though fluid were being injected in one well and produced in the other. Although in reality a single-well experiment would not be producing fluid and tracer in the second well, as long as the injection phase is not long enough for the solute to reach the production well, the result is effectively a single-well simulation. The concentration profile within the system at the end of the injection phase is the initial condition for the backflow phase. The flow is simply reversed for the backflow, with the same inlet and outlet boundary conditions. In the code, the interior concentration values are reversed (C_M switched with C_1, C_{M-1} with C_2, etc.) and the simulation proceeds in the forward direction with an inlet concentration of zero. In this way, a flow model with an inlet and outlet is used to simulate single-well behavior.

An additional feature is the ability to set different velocities, Peclet numbers, and adsorption parameters for the injection and backflow parts of the experiment. This flexibility is necessary to simulate a drift-pumpback experiment, which will typically have different values for these parameters during the two phases of the experiment.

2.5 Code Verification

Although analytic solutions do not exist for all of the modes of operation and parameters required for the reactive tracer study, certain simple cases of the inert and sorbing tracer behavior in which closed-form analytical solutions exist can be used to verify the code. The most useful is the asymptotic solution first derived by Brenner (1962) and reformulated by Satter et al. (1980) for the flow-through

step response of a solute undergoing instantaneous adsorption with a linear adsorption isotherm, assuming the Danckwerts boundary conditions [Eqs. (6) and (7)]. For large Peclet numbers, the following expression is valid:

$$\frac{C^*}{C_{in}} = \frac{1}{2}\,\mathrm{erfc}\,\frac{1-\frac{t^*}{\tau(1+a_L)}}{2\left(\frac{t^*}{\tau(1+a_L)Pe}\right)^{1/2}} - \frac{\left(\frac{t^*}{\tau(1+a_L)\pi Pe}\right)^{1/2}\exp\frac{-\tau(1+a_L)Pe}{4t^*}\left(1-\frac{t^*}{\tau(1+a_L)}\right)^2}{1+\frac{t^*}{\tau(1+a_L)}}$$

$$\cdot\ \frac{1-\frac{6t^*}{\tau(1+a_L)}}{1+\frac{t^*}{\tau(1+a_L)}} - \frac{2\left(\frac{t^*}{\tau(1+a_L)}\right)^2}{\left(1+\frac{t^*}{\tau(1+a_L)}^2\right)}\ , \qquad (14)$$

where τ is the mean fluid residence time, equal to U/L.

Figure 2 compares the step responses of an inert and sorbing tracer (with $a_L = 1$) for Pe = 100 by using Eq. (14) and the finite difference code SORPTION. The finite difference parameters used were $\Delta t = 0.005$ and 101 mesh points. The close agreement indicates that the code is solving the convective-dispersion equation adequately for both inert and sorbing chemical components with an equilibrium adsorption isotherm. The slight discrepancy is attributed to a combination of numerical dispersion in the finite difference approximations and error in the asymptotic solution, which is more accurate at large Peclet numbers. Nonetheless, the agreement is satisfactory, since the maximum discrepancy represents an error of only 5% in estimating the arrival time of a tracer.

The accuracy of the code for a slug injection input can be tested by considering that for an inert tracer or a sorbing tracer with a linear adsorption isotherm, the response to a step change in inlet tracer concentration is simply the integral of the slug response, provided the slug duration is short. Figure 3 shows that for a sorbing tracer with a linear adsorption isotherm ($a_L = 3$ and $b = 0$), the integral of the slug response follows very closely the simulated response to a step change in

inlet concentration. In this case, Pe = 40, Δt = 0.01 and 51 mesh points were used. The slug was injected at C_{in} = 100 for a duration of 0.05. To correct for the finite pulse duration, the time axis was corrected by 0.025, one-half the pulse duration. This allows the curves to be directly compared with the center of the pulse entering the system at t = 0. When this slight effect is corrected for, the simulations agree closely.

These verification simulations prove that the code solves the transport equation properly as long as appropriate finite difference parameters (M and the time step duration Δt) are selected. For several of the simulations presented below, an additional simulation was performed with a finer mesh spacing and time step to verify that the simulations do not exhibit unacceptable errors caused by numerical dispersion. The situations for which no analytic solutions exist to test the accuracy of the code are the nonlinear adsorption isotherms and the injection-backflow experiments. For these cases we must rely on qualitative arguments to verify that the results are correct.

2.6 Simulation of Interwell Experiments

An interwell tracer experiment with an inert solute is used to measure the fluid transit time between the two wells, as well as to characterize dispersion in the system. Figure 4 shows the step response of an inert tracer for different values of Pe. The Peclet number sets the level of tracer spreading but does not significantly affect the mean transit time of the tracer. These curves are nondimensionalized by the mean residence time τ, which for the one-dimensional axial dispersion model equals L/U. Thus, by knowing the path length, the flow velocity may be calculated.

Of course, phenomena not accounted for in this model, such as fracture flow, channeling, and matrix diffusion, will determine the exact shape of a tracer response curve. A more versatile finite difference or finite element transport code must be used to examine these phenonena. A more complex phenomenon that must be considered is the effect of

artificially induced pressure gradients on the fracture flow geometry. Injecting into an injection wellbore to increase the flow velocity between two wells may alter the fracture system in a way that changes the natural flow system. Tracer experiment results under these conditions could be misleading. A series of hydraulic experiments and numerical simulations using more sophisticated numerical simulators must be carried out to quantify this phenomenon.

When a solute molecule undergoes a reversible adsorption reaction with the rock, it reaches the production well later than an inert tracer because it spends part of its stay on the rock surface. Equation (14) indicates that the mean solute residence time $\tau = L/U$ for an inert molecule becomes $\tau(1+a_L)$ for a sorbing tracer with a linear adsorption isotherm. The simulations in Figures 5 and 6 (step change and slug injection, respectively) demonstrate this behavior for different values of a_L. The step response is simply the integral of the slug response for the linear adsorption isotherm. The mean tracer transit time (approximately the peak of the response curve for the slug and inflection point for the step) increases with increasing a_L. Figures 5 and 6 also show a greater apparent tracer dispersion for larger a_L, even though the Peclet number was the same for each case. However, if plotted with a normalized time axis of $t/[\tau(1+a_L)]$ the curves are identical, as implied by Eq. (14).

The range of values for a_L shown in the figures (0.5 to 3) is approximately the range of acceptable equilibrium adsorption isotherm parameters for our field studies. Any stronger adsorption reactions are likely to result in an unacceptably long field experiment. An additional problem with more strongly adsorbing tracers is the large dilution ratios. Since field experiments are almost always slug injections, the outlet concentrations are likely to be very low for a tracer with large a_L.

For interwell tracer experiments employing a solute in the nonlinear portion of the isotherm, the situation becomes much more complicated. Qualitatively, if the concentrations are high enough to be on the flat

portion of the C versus S curve, the rock is essentially saturated with tracer, and the solute will not be significantly delayed by adsorption. If the concentrations are low, adsorption is linear and the response resembles those in the previous section. Figure 7 shows the range of possible types of behavior for a nonlinear, sorbing tracer step response ($a = 1$, $b = 1$) for different inlet concentrations. The mean solute residence time varies with inlet concentration, from a response curve at high C_{in}, which is virtually identical to the inert tracer, to one exhibiting a linear adsorption response with $a_L = 1$ at low concentrations.

Normalized slug response curves are shown in Figure 8 for different slug concentrations. In this comparison, the slug duration is the same, so that 100 times as much material is injected for the $C_{in} = 10$ case. The mean transit time varies with the amount of solute injected in a complex way related to the length of time required for the tracer to be diluted by dispersive mixing. Little or no solute retardation occurs near the injection well. Only after local concentrations reach the level where the isotherm is linear does adsorption become significant. The integrals of these response curves do not equal the step response results since this is a nonlinear phenomenon for which superposition is not valid.

One additional useful comparison is shown in Figure 9, in which the mass of tracer injected is constant for different slug durations. This simulation examines the effect of the sharpness of the spike injected, a variable that is often uncertain in the field because of the various methods of injecting tracer slugs and the dispersive mixing in the wellbore. The response curves are nearly identical, indicating that the mass of tracer injected, and not the concentration of the slug, is the important variable in an interwell tracer undergoing nonlinear adsorption.

In light of these simulations, two possible approaches to designing an interwell sorbing tracer experiment might be considered. We may attempt to use the interesting nonlinear behavior simulated above by designing

experiments in the nonlinear portion of the adsorption isotherm. A comparison of tracer experiments with different injected tracer masses might yield important information on the geometry and mixing characteristics of the flow system. Alternatively, experiments could be carried out entirely in the linear portion of the isotherm. Then the tracer behavior is dependent only on the term a_L, which is related to flowpath properties such as rock surface area to fluid volume ratio or channel aperture width. A comparison of the inert and sorbing tracer responses would provide this important information.

We favor operating the experiment in the linear portion of the isotherm to keep the interpretation as unambiguous as possible. Mixing effects are likely to have a large impact on a tracer undergoing nonlinear adsorption, whereas for linear adsorption these same effects become unimportant. Nonlinear adsorption behavior, though interesting, is dependent on so many unknown geometric properties of the fractured porous medium that experiments would be extremely difficult to interpret.

2.7 Simulation of Single-Well Drift-Pumpback Experiments

The goal of the drift-pumpback experiments using conservative tracers is to measure the natural groundwater flow velocity from a single borehole by determining the rate of migration of a slug of tracer away from the wellbore. Tracer is deposited downhole with a logging tool that breaks a vial containing the tracer. The prevailing groundwater flow field sweeps the tracer from the wellbore into the formation. After a specified length of time (about 1 month), the well is pumped slowly (about 10 to 20 gpm) and water samples are collected and analyzed for tracer. The time required for tracer to appear in the produced fluid can, in theory, be related to the natural flow velocity during the drift phase. Simply put, larger flow velocities during the drift phase of the experiment will result in longer pumpback times before tracer appears.

In this section we examine the applicability of the drift-pumpback experiment for sorbing tracers. Although this form of tracer experiment may be useful for hydrologic characterization, it may not be appropriate for sorbing tracer field studies. The reason is that although the inert tracer response depends primarily on the natural flow velocity in the drift phase and the pumpback rate, the sorbing tracer will also be affected by adsorption in both directions. To recognize the problem that this creates in the simplest possible terms, consider the case of one-dimensional plug flow with no dispersion. Assuming equilibrium adsorption with a linear adsorption isotherm, the distance X traversed by the tracer during the drift phase is

$$X = \frac{U_d t_d}{\tau(1+a_L)} \quad , \tag{15}$$

where U_d is the fluid velocity during the drift phase and t_d is the drift time. During the pumpback, tracer has the same distance to travel as in the forward direction. If the equilibrium adsorption assumption still holds at the higher flow velocity, then the time required for tracer to reach the well during the pumpback is given by

$$t_p = \frac{\tau(1+a_L)X}{U_p} = \frac{\tau(1+a_L)U_d t_d}{U_p \tau(1+a_L)} = \frac{t_d U_d}{U_p} \quad , \tag{16}$$

where U_p is the flow velocity during the pumpback. According to this model, a tracer exhibiting linear, equilibrium adsorption characteristics will return to the well at the same time as the inert tracer and thus provide no new additional information.

Clearly, more sophisticated modeling must be performed to examine the effects of dispersion and sorption reaction kinetics before discounting the drift-pumpback experiment for adsorbing tracers. Figure 10 shows the results of a 1 month drift-pumpback tracer experiment employing four tracers injected initially and after 1, 2, and 3 weeks. The internal concentration profiles of a drifting tracer are shown in Figure 11. As

the tracer drifts, it also undergoes dispersion, so upon returning to the well during the pumpback, the response depends on both how far it drifts and the level of dispersion encountered.

A more subtle effect caused by axial dispersion is demonstrated in Figure 12. For Pe = ∞, the tracer returns as a perfect spike at time equal to $t_p U_d / U_p$. However, for a finite level of axial dispersion, the peak response occurs at an earlier time. The level of dispersion affects the peak response time as well as the shape of the response curve. Although valid objections can be made against the one-dimensional axial dispersion equation for modeling dispersion in underground flow systems, this calculation illustrates the importance of formulating an accurate flow model to interpret tracer dispersion, even for this conceptually simple tracer experiment.

Figure 13 shows a series of drift-pumpback sorbing tracer simulations for a linear adsorption isotherm with different values of a_L. Our earlier arguments suggested that in the absence of dispersion the tracers should return to the well simultaneously. However, the peaks in Figure 13 arrive at the well earlier for larger values of a_L. This seeming contradiction can be resolved by noticing the qualitative similarity of these curves with those of Figure 12, the inert tracer drift-pumpback experiment. A larger value of a_L gives rise to what is in effect a dispersion phenomenon. Just as in the flow-through simulations, adsorption results in a larger apparent tracer dispersion. In the drift-pumpback experiment a greater degree of tracer spreading is accompanied by an earlier arrival of tracer to the wellbore, whether that spreading is due to greater fluid dispersion or sorption.

Since different response curves are obtained for different values of a_L, the drift-pumpback sorbing tracer experiment can in theory provide important flow information. In this case the shape of the response curve, rather than simply the mean arrival time, is compared to that of an inert tracer. Thus the response is more intimately related to the specific flow geometry and mixing patterns of the fracture system, making the experiment more difficult to interpret. If the number of

reactive tracer experiments is limited, interwell experiments probably should be selected, since they appear to be preferable to drift-pumpback experiments. However, since inert tracer drift-pumpback experiments are already scheduled, at least one drift-pumpback sorbing tracer experiment should be considered to evaluate the concept. Notice also that experiment duration and concentration level are relatively insensitive to the value of a_L. Thus, we are not as limited in our choice of tracers. More strongly sorbing tracers may be acceptable in this mode of operation. This could make the job of finding appropriate sorbing tracers easier.

In the time scale of an interwell sorbing tracer experiment, kinetics effects will probably not be important, as the reaction should proceed to equilibrium in a time that is short compared to the overall transit time between the wells. However, the pumpback phase of the drift-pumpback experiment will last on the order of minutes or hours, making kinetics effects potentially very important. The current model cannot simulate adsorption kinetics phenomena except for the extremes of equilibrium or no adsorption. Figure 14 shows model results assuming equilibrium adsorption in the drift phase and no adsorption in the pumpback portion of the experiment. A more strongly adsorbing tracer stays closer to the wellbore and thus returns earlier in the absence of adsorption during pumpback. The reason the total recovery of tracer is less for larger a_L is that the model as currently formulated assumes that the adsorbed tracer at the end of the drift remains on the rock indefinitely. When adsorption kinetics are incorporated into the code, this problem will be resolved and more realistic behavior will be simulated.

Most importantly, kinetics effects are more likely to be present in a drift-pumpback sorbing tracer experiment because of the short pumpback times. Thus, in addition to equilibrium adsorption parameters, laboratory kinetics data must be collected for potential drift-pumpback tracers before field experiments are performed. This additional

complication and the more difficult interpretation of a field experiment make drift-pumpback sorbing tracer testing less desirable than interwell experiments.

Chapter 3. Modeling in Support of Laboratory Tracer Studies

3.1 Introduction

So far, the primary focus of the modeling studies has been the simulation of the likely behavior of field experiments and identification of potential problems with the different proposed operating modes. Another goal of our preliminary modeling is to provide information necessary to design the laboratory experimental work. This chapter outlines our modeling effort designed to determine what type of information is required about the equilibrium sorption parameters, mechanisms, and kinetics. The first section describes the desirable properties for a reactive tracer and outlines the types of laboratory sorption measurements required, and the remaining sections address the issue of reaction kinetics.

3.2 Desirable Sorption Parameters and Properties

The sections on modeling the interwell and drift-pumpback tracer experiments identified appropriate sorption parameters for obtaining useful field information. For interwell experiments the range of appropriate values of a_L in the Langmuir model is about 0.5 to 3, whereas drift-pumpback experiments could usefully be performed with values of a_L as high as 10. For linear adsorption in a homogeneous medium, a_L is related to the more familiar equilibrium distribution coefficient K_d by the following expression:

$$a_L = \frac{\rho_b K_d}{\phi} \tag{17}$$

where

$$K_d = \frac{m_r V_l}{m_l w_r} \quad . \tag{18}$$

In these expressions, ρ_b is the bulk rock density, ϕ is the porosity, m_r is the mass of tracer residing on the rock, m_l is the mass of tracer residing in the fluid, V_l is the liquid volume, and w_r is the rock mass.

As shown earlier, another desirable quality of the reactive tracer is a linear adsorption isotherm over the concentration range of the tracer in the field experiments. If this is not true for a given tracer, the isotherm must be known accurately in the concentration range of interest. This range is dependent on the measurement sensitivity of the tracer, the method for injecting the tracer, and the dispersive characteristics of the medium. Though it is impossible to predict these factors a priori, some general guidelines can be outlined. To design a field experiment, the tracer mass injected is selected so that the peak concentration is at least 1 order of magnitude higher than the lowest concentration that can be measured accurately. This concentration is governed either by the measurement sensitivity of the chemical analysis technique or by the need to be significantly above the background concentration of tracer. Near the injection well, the concentrations will be much larger until the concentrated tracer pulse has been diluted by dispersive mixing. Dilutions of at least 3 orders of magnitude from the concentration of the injected slug are usually observed.

Thus, the isotherm should be measured over 4 orders of magnitude starting at the lowest measurable concentration. If a tracer exhibits unwanted nonlinear behavior at higher concentrations, the method for injecting tracer into the formation could be designed to keep the concentration lower. This could be done by using a more dilute square wave concentration input instead of a highly concentrated pulse of solute.

Surface area should also be considered in laboratory screening experiments. The physical significance of the variable a_L in a sorbing tracer experiment depends on the nature of the medium. The solute mass balance implies that for a linear adsorption isotherm,

$$a_L = \frac{m_r}{m_l} \quad . \tag{19}$$

In a homogeneous porous medium, the expression for a_L given in Eq. (17) is appropriate. K_d is determined in batch reactor experiments by allowing a solute to come to equilibrium with a sample of reservoir rock and measuring the relative amounts of the solute on the rock and fluid at equilibrium. All considerations of the effect of surface area are eliminated by employing a representative rock sample with the same specific surface area (surface area per unit mass of rock) as the underground porous medium.

One of the weaknesses of this approach is that many porous media contain fractures or channels that can conduct a majority of the fluid and solute. For this reason the one-dimensional model developed in Chapter 2 used a sorption model based on rock surface area rather than rock mass. For solute transport through fractures, a more convenient formulation for the term a_L is

$$a_L = a^* K_f \quad , \tag{20}$$

where K_f is the surface sorption equilibium constant, given by

$$K_f = \frac{m_r V_l}{m_l S_r} \quad ; \tag{21}$$

K_f is obtained from K_d by dividing by the specific surface area of the rock.

Equation (20) implies that the determination of a_L in a field experiment allows us to calculate a^*. For flow through a smooth fracture,

$$a^* = \frac{2}{w} \quad , \tag{22}$$

where w is the fracture aperture. Therefore, field experiments with sorbing tracers can in theory provide values for fracture apertures, an additional piece of information not obtainable from inert tracer

experiments. In practice, the solute will encounter a distribution of apertures, and the tracer response must be interpreted by using more complex models.

This analysis suggests that the batch sorption reaction studies should address the effect of surface area. In crushed particle experiments, the surface area must be determined, preferably by both a particle size distribution calculation and with BET measurements. In addition, the tracers should be tested at at least two different particle sizes to determine whether the theoretical first-order dependence of sorption on a^* is valid.

Finally, the presence of alteration minerals lining the fractures should be addressed in the laboratory experiments. If the flow is fracture dominated, sorption will be controlled by solute-mineral interactions on the fracture faces, which may be different from reactions with the crushed particles obtained from drill cuttings or cores. A batch experiment using minerals thought to be deposited on the fracture faces in the saturated zone would answer this question.

3.3 Kinetics Effects

One phenomenon not explicitly treated in the one-dimensional model was adsorption kinetics. The reaction was assumed to occur instantaneously at all positions, creating local equilibrium between the tracer residing on the surface and in the liquid. The adsorption isotherm, or surface concentration versus liquid concentration curve, defines the interaction between tracer and rock.

Reactions need not occur instantaneously, however. Depending on the rate of sorption reaction and characteristic residence time of fluid and tracer, a tracer with a given equilibrium adsorption isotherm may undergo equilibrium adsorption, no adsorption, or some state in between these two extremes. This fact requires that laboratory adsorption kinetics data be acquired, or that it otherwise be shown that reaction rates are rapid. In a field experiment, equilibrium adsorption may be

assumed only when the characteristic reaction time is much smaller than the typical fluid residence time. This time will be different for the interwell and drift-pumpback modes of operation. This section outlines the usual approach for modeling kinetics effects, and the last section of this chapter estimates the C-wells fluid residence times for a typical tracer experiment, thus providing time scales for laboratory experiments for examining kinetics and sorption equilibria.

To illustrate the importance of kinetics, the one-dimensional model developed in Chapter 2 for equilibrium adsorption will now be revised to include adsorption kinetics. For Langmuir adsorption kinetics, dimensionless groups are identified that govern whether adsorption kinetics are important. The choice of the Langmuir model is not important here: for any proposed adsorption model, the importance of reaction rates can be shown from the model.

As in Section 2.2, the one-dimensional, transient axial dispersion equation is employed. Since equilibrium adsorption was assumed, an analytic expression relating C* and S* was possible, which was used to eliminate surface concentration from Eq. (2). However, for rate-controlled adsorption, an additional differential equation must be introduced. To be consistent with the previous modeling, a kinetic Langmuir adsorption model is assumed:

$$\frac{\partial S^*}{\partial t^*} = K_{s1} \left(1 - \frac{S^*}{S_s^*}\right) C^* - K_{s2} \frac{S^*}{S_s^*} \quad . \tag{23}$$

The first term on the right-hand side represents the rate of adsorption and is proportional to the liquid concentration and the fraction of available adsorption sites. The second term is the rate of desorption, which is proportional to fractional coverage of tracer on the available adsorption sites. The three parameters in the model are the adsorption rate constant K_{s1}, the desorption rate constant K_{s2}, and the maximum surface concentration S_s^*. At large times, the Langmuir adsorption isotherm is obtained.

Nondimensionalizing Eqs. (2) and (23), we obtain

$$\frac{\partial C}{\partial t} + N_A \frac{\partial S}{\partial t} = Pe^{-1} \frac{\partial^2 C}{\partial x^2} - \frac{\partial C}{\partial x} \quad , \tag{24}$$

and

$$\frac{\partial S}{\partial t} = K_1(1-S) - K_2 S \quad , \tag{25}$$

where $S = S^*/S_s^*$, and the additional dimensionless groups and variables are defined below:

$$N_A = \frac{a^* S_s^*}{C_{ref}} \quad , \tag{26}$$

$$K_1 = \frac{K_{S1} L C_{ref}}{U S_s^*} \quad , \text{ and} \tag{27}$$

$$K_2 = \frac{K_{S2} L}{U S_s^*} \quad . \tag{28}$$

The key parameters governing the importance of adsorption kinetics are K_1, the dimensionless rate constant of adsorption; K_2, the dimensionless rate constant of desorption; and N_A, the adsorptive capacity. The kinetics parameters are ratios of the fluid residence time to the characteristic reaction time. When they are much greater than 1, equilibrium adsorption may be assumed. When either term is of order 1, kinetics cannot be neglected. The adsorptive capacity compares the maximum quantity of tracer adsorbed to the typical quantity residing in the liquid phase. When N_A is large, the fractional rock surface coverage $S = S^*/S_S^*$ will be low.

Thus, to evaluate possible kinetics effects in a field experiment, we must compare the characteristic sorption and desorption reaction times to the probable fluid residence time in the field experiments. The dimensionless groups K_1 and K_2 were defined above for the Langmuir adsorption model. In general, a dimensionless group K_r for any kinetic adsorption model can be defined by

$$K_r = \frac{\tau_f}{\tau_r} \quad , \tag{29}$$

where τ_f is the characteristic fluid residence time and τ_r is the characteristic of adsorption reaction time. When K_r is much greater than 1, equilibrium can be assumed and kinetics effects are negligible.

3.4 Estimated Fluid Residence Times

To screen potential tracers in the laboratory, we must be sure that the kinetics of adsorption are studied in the proper range of residence times. Otherwise, unwarranted extrapolations will be required to apply laboratory results to field studies. This section examines the possible residence times for different proposed tracer experiments at the C-wells. Since these estimates cannot be verified without a conservative tracer experiment, laboratory experiments should cover a wider range of times to ensure that when tracer experiments are performed, valid laboratory data are available in the range of interest.

An estimate of fluid transit time in an interwell tracer experiment will be made by calculating a likely fracture void volume and dividing by injection flow rate. The following wellbore separation distances have been determined for the C-wells:

C1-C2: 77 m (252 ft),
C1-C3: 68 m (224 ft), and
C2-C3: 30 m (100 ft).

Despite the likelihood of anisotropic permeability in a fractured medium, let us assume that fluid injected into C1 travels radially away from the injection point. Tracer will reach the C2 and C3 monitoring boreholes after sweeping the pore volume from a disc-shaped region of rock with a radius of 77 m and a thickness of 30.5 m (100 ft, an order of magnitude estimate of reservoir thickness). This rock volume of 5.68×10^5 m^3, multiplied by an assumed fracture porosity of 10^{-3}, yields a fracture pore volume of 568 m^3. At a typical injection flow rate of 6.3×10^{-3} m^3/s (100 gpm), the estimated fluid travel time is 25 h.

The drift-pumpback tracer experiment requires travel time estimates for both phases of the experiment. The drift-phase time must be long enough that the tracer moves out of the near-wellbore region and into the main body of the fracture system. If we assume this distance is about 10 m, and use a linear flow velocity estimate of 0.15 m/day, we obtain a drift-phase duration of about 2 months.

The pumpback duration may be calculated by assuming radial inflow of tracer from a distance of 10 m through a zone 9 m thick (30 ft, a typical packed-off wellbore distance). If we assume the same fracture porosity of 10^{-3} and a flow rate of 6.3×10^{-4} m^3/s (10 gpm), the estimated backflow time is about 75 min.

Obviously, these calculations are based on very rough estimates of tracer transit times. When better information becomes available, we will make new estimates. Nonetheless, they probably bracket the range of times over which kinetics effects must be tested. If only interwell experiments are planned, kinetics experiments must cover the range of times from zero to several days. For drift-pumpback experiments, however, kinetics experiments should be carried out for at least 2 months to ensure that long-term kinetics effects are not occurring during the drift phase. Furthermore, early-time data in the first hour of the laboratory experiment must be obtained accurately to characterize sorption during the pumpback phase, which would only last several hours. This additional requirement must be considered when deciding whether to develop tracers for drift-pumpback as well as interwell experiments.

Chaper 4. Residence Time Distribution Modeling

4.1 Introduction

So far we have examined only the simple one-dimensional axial dispersion model for performing preliminary scoping calculations. In reality, the tracer-determined residence time distribution (RTD) in fractured media is much more complex than can be described by dispersion in a one-dimensional flow field. This chapter outlines a modeling approach that uses the measured inert tracer RTD as input to mixing models capable of simulating transient reactive tracer data. This model can eventually be used to interpret field data, so it could also properly be included in the chapter on code development. However, here we use the mixing model for preliminary simulations using typical conservative tracer responses in fractured media. Therefore, we include the model development and simulations here.

4.2 Description of RTD-Based Models

One axiom of modeling flow and transport in porous media is that a variety of models can match the observed data and yet still yield different predictions of some other facet of behavior. This nonuniqueness problem must be confronted in any modeling study. The field of chemical reaction engineering has dealt with this difficulty for modeling the extent of chemical reaction in continuous flow chemical reactors by devising flow models that place bounds on the result, rather than providing an exact solution. For example, by knowing the batch reactor kinetics and conservative tracer RTD for the flow system, the extent of reaction may be calculated exactly for a first-order reaction. Furthermore, close bounds on conversion can be obtained for reactions with nonlinear kinetics by using mixing models that match the tracer RTD for different well-defined flow geometries.

The fundamental principle used in these so-called micromixing models is that models that match the conservative tracer RTD differ only in the earliness or lateness of mixing of molecules of different residence time, which gives rise to different behavior for solutes undergoing nonlinear processes. The two extremes of micromixing are depicted in Figures 15 and 16. The latest possible backmixing or minimum mixedness occurs when the RTD is represented by a network of plug flow reactors connected in parallel. Fluid and tracer of different residence times remain unmixed until they reach the outlet manifold. The volumes and flow rates of each path are adjusted to approximate the measured conservative tracer response. The maximum mixedness reactor is a plug flow reactor with side entrances whose positions and flow rates are also adjusted to match the RTD. However, since fluid mixes with other fluid of longer residence times immediately upon entering the system, the system has the earliest possible mixing of fluid of different residence times.

Given a conservative tracer response, these models can predict the extremes of sorbing tracer behavior. In addition, they can be used to predict tracer behavior for different tracer inputs such as slug, step injection, or slug injection with recirculation. This chapter develops the mathematics of the maximum mixedness model (Figure 15) and uses the model to perform scoping calculations for typical two-well conservative tracer responses in fractured media. The minimum mixedness model (Figure 16) is considerably more difficult to simulate numerically and at the present time is not ready for use.

4.3 Mathematical Description of the Maximum Mixedness Model

Zwietering (1959) developed the mathematics of the maximum mixedness model for the case of flow and homogeneous chemical reaction in the fluid phase, thus providing a bound on the steady-state chemical reaction conversion in a reactor of arbitrary conservative tracer RTD. Here we summarize Zwietering's result and then alter the mass balance to describe sorption for a Langmuir adsorption isotherm. From RTD theory, the conservative tracer response is normalized by using $f(t) = QC(t)/m_p$,

so that f(t)dt is the fraction of fluid leaving the flow system with residence times between t and t + dt. The cumulative RTD $F(t) = \int_0^t f(t)dt$ is the fraction of fluid leaving the system with residence times of t or less. Next, we define the life expectation of a molecule λ as the length of time remaining before a molecule is due to leave the system. In the maximum mixedness model, λ is clearly 0 at the outlet and increases at increasing distances into the plug flow reactor. Thus λ is equivalent to a position in the plug flow reactor.

Zwietering showed that the concentration mass balance for the model with chemical reaction is

$$\frac{\partial C^*}{\partial t^*} = \frac{\partial C^*}{\partial \lambda} - \frac{f(\lambda)}{1-F(\lambda)} \left(C^* - C^*_{in}(t^*)\right) + R(C^*) \quad , \tag{30}$$

where $R(C^*)$, the chemical reaction term, is, for example, $-kC^*$ for a first-order reaction and $-kC^{*2}$ for a second-order reaction. The boundary conditions are the inlet concentration C^*_{in} and $\partial C^*/\partial\lambda = 0$ as λ goes to ∞. The desired solution is the outlet concentration at $\lambda=0$.

In the present study we are concerned with adsorption rather than chemical reaction, so $R(C^*) = 0$. Also, whereas Zwietering was concerned only with the steady-state solution of Eq. (30), we require transient solutions for given time-dependent input functions $C^*_{in}(t^*)$. The Langmuir adsorption isotherm may be incorporated into the mass balance exactly as with the axial dispersion model, the result being

$$1 + \frac{a_L}{(1+b_2C^*)^2} \frac{\partial C^*}{\partial t^*} = \frac{\partial C^*}{\partial \lambda} - \frac{f(\lambda)}{1-F(\lambda)} \left(C^* - C^*_{in}(t^*)\right) \quad . \tag{31}$$

This equation can be solved by finite difference to obtain the internal concentration profile and, more importantly, the outlet concentration as a function of time. The reactor is discretized in the spatial or λ direction from the input values of the inert tracer RTD. Thus the number of finite difference cells in the reactor equals the number of data points in the RTD f(t). Then, letting $N(\lambda) = f(\lambda)/(1-F(\lambda))$, the finite difference approximation to Eq. (31) is

$$\frac{\partial C_i^*}{\partial t^*} = \frac{1}{1 + \frac{a_L}{(1+b_2 C^*)^2}} \quad \frac{C_i^* - C_{i+1}^*}{\Delta\lambda} - N(\lambda)\left(C_i^* - C_{in}^*(t)\right) = g[C_i^*(t)] \quad . \tag{32}$$

The boundary condition at large λ is applied at the last position in the reactor, resulting in

$$\frac{\partial C_M^*}{\partial t^*} = \frac{1}{1 + \frac{a_L}{(1+b_2 C_M^*)^2}} \quad N(\lambda)(C_M^* - C_{in}^*(t)) = g[C_M^*(t)] \quad . \tag{33}$$

Using a Crank-Nicolson time integration scheme, we obtain

$$C_i^*(t+\Delta t) = C_i^*(t) + \beta\Delta t^* g[C_i^*(t+\Delta t^*)] + (1-\beta)\Delta t^* g[C_i^*(t)] \quad . \tag{34}$$

The equation set is solved by using a Gauss-Seidel iterative procedure that successively solves Eq. (34) until the solution exceeds a user-selected convergence criterion. One version of the code calculates the tracer response for either a step change or a pulse concentration input, assuming no recirculation of the produced fluid. A second code simulates a pulse injection but then uses the outlet concentration as the inlet to the reactor, thus simulating the two-well recirculating case.

4.4 Code Verification

The code is easily verified by using the exponential RTD of a continuous stirred tank reactor (CSTR):

$$f(t^*) = \frac{1}{\tau} e^{-t^*/\tau} \quad . \tag{35}$$

For a step change input of a conservative tracer, the outlet concentration should be

$$\frac{C^*}{C_{in}^*} = 1 - e^{-t^*/\tau} \quad . \tag{36}$$

Figure 17 shows the close agreement between the maximum mixedness model result (the curve) and the results calculated from Eq. (36) (the x's). To verify the recirulating tracer response, we use the fact that for the well-mixed CSTR, recirculation should immediately result in a constant concentration at the outlet. In Figure 18, tracer is injected from time 0 to 0.4, at which time recirculation begins. The concentration abruptly becomes constant, thus verifying the model for recirculation of a conservative tracer. Finally, calculations similar to Figure 17 for a sorbing tracer with b = 0 results in a similar response but with an exponential time constant of $\tau(1+a_L)$, as expected.

4.5 Maximum Mixedness Model Results

To demonstrate the likely behavior of C-wells sorbing tracer experiments, we require an inert tracer response in a two-well tracer experiment in fractured rock. Since C-wells conservative tracer data do not yet exist, we employ two conservative tracer experiments in fractured geothermal reservoirs at the Fenton Hill, NM, Hot Dry Rock geothermal energy site. The first, Experiment 217-A2 (Robinson and Tester, 1984) is shown in Figure 19 and the second, Experiment 2067-T2 (Robinson et al., 1987) is shown in Figure 20. The two response curves have the characteristic shape of an early elevated response caused by channeling through direct flow paths and a long tail representing flow through an indirect labyrinth of fractures connecting the wells. The fracture system of 217-A2 has relatively more channeling and less long-residence-time flow paths than that of 2067-T2. For these preliminary calculations, we assume that these tracer curves are similar to results that will be obtained at the C-wells.

The predicted sorbing tracer responses for a linear adsorption isotherm ($b_2 = 0$) for different values of a_L are shown in Figures 21 and 22. The simulations for 217-A2 (with greater channeling) resemble those of the axial dispersion model, with the peak response shifted to longer residence times. This behavior is also present in 2067-T2, but the predicted concentrations of sorbing tracer stay below that of the conservative tracer except at very long residence times. This result

illustrates the importance of the internal flow patterns and inert tracer RTD in determining the nature of the sorbing tracer response. Models such as the maximum mixedness model or more conventional finite difference or finite element codes must first accurately represent the conservative tracer response before being used to simulate sorbing tracer behavior.

The recirculating version of the maximum mixedness code can illustrate the ramifications of reinjecting tracer in a two-well recirculating tracer experiment. The effects of recirculation on the conservative tracer responses are shown in Figures 23 and 24. In each case the information in the tail of the response curve is completely masked by reinjection of produced tracer, and in 217-A2 this even affects the peak tracer response time and height. Similarly, sorbing tracer responses are adversely affected to the point that interpretations could be hampered by recirculation (Figure 25). Although numerical deconvolution techniques can be used to account for reinjection of produced fluid tracer (Robinson and Tester, 1984), this approach results in greater model uncertainty and can be avoided with proper water management. Produced fluid should not be reinjected. Instead, water containing tracer should be stored or disposed of at the surface and fresh water should be injected. Alternatively, the tracer could be removed from the water before reinjection. This method depends entirely on the tracer selected and will often be very difficult to accomplish in real time.

Finally, the maximum mixedness model can be used to simulate one extreme of sorbing tracer behavior for nonlinear sorption. To understand why only bounds are possible rather than an exact solution for nonlinear adsorption, consider Figure 26, where two elements of fluid are at fluid and surface concentrations denoted by points A and B. If these two elements of fluid mix immediately upon entering the system, the new fluid has an intermediate concentration denoted by C. If they remain unmixed and travel through the system, the average amount of sorption is given by point D. The early mixing or maximum mixedness case results in greater total adsorption than if the molecules remain unmixed until the exit. This result is generalized by observing that for sorption

isotherms that are concave down, early mixing increases the overall adsorption; for a linear isotherm the earliness of mixing has no effect on sorption. A linear isotherm is thus more desirable since it eliminates one source of uncertainty in the model results.

Nonetheless, it may be impossible to identify a tracer with linear sorption characteristics over the entire range of concentrations encountered, particularly since in field experiments short slugs of high concentration are usually injected. Thus the effects of nonlinear adsorption should be examined. Figure 27 shows the maximum mixedness extreme for a nonlinear sorbing tracer ($a_L = 1$, $b_2 = 1$) for different injection concentrations. The tracer undergoes almost no adsorption at high injection concentrations (C_{in} = 1000 or higher) and behaves as a tracer with a linear isotherm for lower concentrations (C_{in} = 10 or less). Although the minimum mixedness model is not yet developed, the results will probably show a similar family of response curves but at concentrations about 2 orders of magnitude lower. In other words, when mixing and dilution of the injected slug do not occur until the outlet, much lower injection concentrations are required to prevent nonlinear sorption effects (curves 2 and 3). Of course, more detailed modeling of these effects is premature since we have not yet identified a tracer and determined its adsorption isotherm. When a tracer is selected, RTD modeling can then be used to design the experiment to minimize nonlinear effects or, if they are unavoidable, to assess their importance.

Chapter 5. Development of Models for Interpreting Field Experiments

5.1 Introduction

A combination of existing codes and models currently being developed will be used to simulate the C-wells conservative and sorbing tracer experiments. This chapter briefly summarizes the existing codes that will be used for future pre-experiment scoping calculations and postexperiment modeling. Then, the use of RTD-based models (Chapter 4) for interpreting field experiments is described. Finally, in the remaining sections of this chapter, a new fracture network model being developed is discussed in greater detail.

5.2 Currently Available Codes

A finite difference code, TRACR3D (Travis, 1984) and a finite element code, FEHM (Zyvoloski, 1983), will be used to examine different aspects of the C-wells tracer experiments. Both codes can solve the fluid mass and momentum conservation equations necessary before obtaining a tracer solution. TRACR3D is well suited for solving the solute transport equation for both conservative and reactive species, with the provision for either an equilibrium or kinetics formulation for adsorption. FEHM will require some additional development if it is to be used for sorption, but it has certain advantages over TRACR3D. Since it solves the energy balance equations, it can assess temperature effects as well as model temperature logs within wellbores, an important piece of data in hydraulic field experiments. Also, FEHM can model the case of permeability changes with pressure, a potentially important phenomena in injection experiments in fractured media.

Although both codes have the provision for including fractures in the flow domain, neither is practical when attempting to simulate flow through a large number of fractures. Thus these codes will be used to simulate temperature and flow information from hydraulic experiments and to perform preliminary calculations for planning the tracer experiments.

Then, to model the experiment results, they will be used in a continuum modeling approach to determine the applicability of assuming an equivalent porous medium for fluid flow and tracer transport at the C-wells.

5.3 Residence Time Distribution Modeling

In Chapter 4, the usefulness of RTD-based transport modeling was demonstrated for obtaining solute transport predictions in a closed-flow system with a known conservative tracer RTD. Bounds on the possible types of behavior can be obtained for a given conservative tracer response curve. Thus, without knowing the details of the internal flow structure between two wells, we can model the sorbing tracer response curve and obtain valuable information about transport processes with these models.

However, enhancements to these RTD-based models must be developed before they are useful for modeling field experiments. The simulations in Chapter 4 assumed constant sorption properties, independent of position. The RTD-based models can account for sorption variability within the flow domain by making the sorption parameters a function of residence time. This amounts to saying that the short-residence-time flow paths have a certain characteristic sorption and the long-residence-time paths have another, possibly different behavior. Another phenomenon not presently accounted for is sorption kinetics, which can be included by solving a differential equation describing the kinetics simultaneously with the flow equation. When these revisions are complete, the RTD-based models will provide an alternative approach to solute transport modeling in porous media.

5.4 Rationale of Fracture Network Modeling

Reservoir engineers and groundwater hydrologists have long recognized the importance of fractures on fluid flow and solute transport in underground porous media. Analytical and numerical models exist to predict flow behavior for various fracture geometries ranging from a

single fracture to multiple, interconnected fractures. Solute transport is not so easily simulated by these simple models, however. The typical approach of employing the convective-dispersion equation with the adjustable parameter of dispersion coefficient is usually inadequate. Multidimensional forms of the convective-dispersion equation can often provide good fits, but at the expense of adding more adjustable parameters of questionable physical significance. Furthermore, the fundamental assumption of a homogeneous porous medium may be incorrect for a fractured porous medium unless it is very highly fractured.

Fracture network modeling is a different approach to simulating flow and transport in fractured porous media. The flow system is assumed to be composed of a network of interconnected fractures. A pressure difference imposed in such a system because of fluid injection or a natural hydraulic gradient results in a flow of water through the fractures. This flow field can be calculated by assuming a fracture geometry, appropriate pressure/flow boundary conditions, and a relationship between pressure drop and flow rate within each fracture. Once the flow field is determined, the transport of a conservative, reacting, or adsorbing chemical component can be calculated by using particle-tracking techniques, which follow the progress of a representative sample of tracer molecules through the network.

Fracture network modeling has been used extensively in the past to model groundwater flow [see, for example, Castillo et al. (1972), Schwartz (1977), Smith and Schwartz (1980), Schwartz et al. (1983), Long et al. (1982), Andersson and Thunvik (1986), Hopkirk et al. (1985), and Karasaki (1986)]. The primary focus of most previous work has been to determine the conditions under which a fractured medium could be treated as an equivalent porous medium. With the fracture network approach, one can assess the effect of fracture size, spacing, aperture, and orientation on the fluid flow, permeability distribution, and tracer behavior. Typically, Monte Carlo techniques are used, in which a large number of realizations of different fracture geometries, all with identical fracture statistics, are performed to determine the average and variability of behavior. The latter is a measure of the inherent

uncertainty of flow behavior in the fracture network, given the measured statistical parameters. These studies have usually restricted flow to a rectangular grid in two dimensions, with constant-head boundary conditions at opposite ends of the plane and no-flow or linearly decreasing head boundaries on the two sides. These boundary conditions simplify the analysis and interpretation of results and are appropriate for modeling large-scale groundwater flow problems.

Unfortunately, interwell flow and tracer experiments such as those proposed for the C-wells cannot be interpreted with these simplified boundary conditions. Wellbores often resemble point sources and sinks for flow, as they are directly connected to only a few fractures. Karasaki (1986) has examined the effect of the wellbore boundary condition with a finite element fracture network code that solves the transient pressure diffusion equation in the fracture network. The code FRACNET being developed for use in the C-wells sorbing tracer project is suitable for a steady-state flow field established from a single-flow field or between an injector and producer in an interwell experiment. Having realistically simulated the flow field in a fractured medium under pumping stress, the code will then be used to model transport processes. Particle-tracking techniques currently being developed will handle the diverse phenomena of conservative tracer behavior, matrix diffusion, and sorption.

5.5 Development of FRACNET Code

Fracture Network Generator: A fracture network generator has been developed to simulate steady-state flow from a single wellbore or between two wellbores. A two-dimensional, interconnected network of fractures is generated within a circular region of arbitrary diameter, which serves as the outer boundary. This boundary is currently a no-flow boundary, but a future option will allow it to be set as a constant-pressure boundary. Wellbores are simulated as constant-pressure line segments within the region.

The fracture network generating technique is similar to that of Long et al. (1982). A network consists of two sets of fractures, each with a preferred orientation. A fracture is located randomly in space, and then its direction, length, and aperture are selected from random distributions. An example of a fracture network with two wellbore line segments is shown in Figure 28.

When all fractures are generated, the code then determines the intersection points of each fracture with other fractures, the wellbores, and the outer boundary. This information is contained in a connectivity matrix that for each node stores the node numbers of all nodes connected to it. Also stored is the aperture and flow length information necessary to solve the pressure field and tracer solutions. Finally, a technique has been devised to eliminate nodes or groups of nodes that are not connected to the rest of the network or that are connected only through one node, and hence are dead-end pathways. The resulting connected node network for the fracture network of Figure 28 is given in Figure 29.

Fluid Flow Law: If we assume that fracture flow can be modeled as laminar flow between parallel plates separated by distance w, the fracture aperture, the fluid velocity is given by

$$U = \frac{-w^2 \Delta P}{12 \mu L} \quad , \tag{37}$$

where P is pressure and μ is fluid viscosity. The volumetric flow rate per unit depth of fracture is

$$q = wU = \frac{-w^3 \Delta P}{12 \mu L} \quad . \tag{38}$$

The sign convention is such that flow into a node is positive, and flow from a node is negative.

Flow Equations: As noted by Castillo et al. (1972), the least number of unknowns results when an equation is developed for the pressure at each node. This approach eliminates the need to define mesh points within each fracture. The fluid mass balance at each node is

$$\sum_{i=1}^{n} q_i = \sum_{i=1}^{n} \frac{w_i^3 (P_i - P_o)}{12\mu L_i} = 0 \quad , \tag{39}$$

where n can be 2, 3, or 4, depending on the number of fractures connected to the node. By rearranging Eq. (39),

$$P_o = \frac{\sum_{i=1}^{n} \frac{w_i^3 P_i}{L_i}}{\sum_{i=1}^{n} \frac{w_i^3}{L_i}} \quad , \tag{40}$$

where subscript o represents the node in question and the i's refer to the adjacent nodes. Equation (40) is an expression for the pressure at node o in terms of pressures at the adjacent nodes.

Solution of Flow Equations: Equation (40) can be written for the pressure at each node, and the pressure of the source and sink nodes is set constant. The outer boundaries automatically simulate the no-flow condition because they are not connected to any points on the other side of the boundary. The resulting equation set is solved by using the successive overrelaxation (SOR) method, an iterative solution procedure that offers a considerable improvement over the successive substitutions or Gauss-Seidel techniques. By optimizing the numerical parameter ω, the solution vector more rapidly approaches the correct values for slowly converging equation sets. A value of 1.87 was found to be optimum for a test problem, decreasing the number of iterations by a factor of 8 over the Gauss-Seidel method ($\omega = 1$).

Particle-Tracking Technique: The assumption underlying the particle-tracking technique is that a tracer response can be approximated by passing a large number of individual tracer molecules through the system, measuring the residence time of each, and

accumulating the overall response as the RTD of the individual molecules. The technique assumes that the transport processes are independent of the concentration of tracer: each molecule is a separate entity exerting no influence on other tracer molecules.

To calculate the residence time of an individual molecule traveling from the source to the sink, the residence time within a fracture must first be determined, and then an appropriate rule governing tracer transport at a node must be assumed. Within a fracture, assume that τ_c, the residence time of a conservative tracer, is simply the length divided by the average fluid flow velocity, or

$$\tau_c = \frac{-12\mu L^2}{w^2 \Delta P} \quad . \tag{41}$$

This simplification implies no dispersion within a fracture. Robinson and Tester (1984) have shown that dispersion within a fracture is small compared to overall dispersion levels in heterogeneous media. At a fracture intersection, we assume complete mixing, so the tracer partitions to the different fractures in the same proportion as the flow rate. In the particle-tracking formulation, the probability that an individual molecule at a node chooses a given fracture is equal to the flow fraction entering that fracture. A random number generator is used to choose which path a molecule takes. When the particle reaches the sink, the total residence time is the sum of the residence times in the individual fractures.

When this calculation is repeated, say 10,000 times, a distribution of residence times is obtained. To record the tracer response, a group of time blocks (0 to Δt, Δt to $2\Delta t$, $2\Delta t$ to $3\Delta t$ ...) is identified and the number of molecules with residence times falling in each of the time blocks is counted. The resulting histogram is the RTD f(t), equivalent to the response of the system to a short slug of tracer injected at the inlet. The integral of this function, when normalized to unity, is the cumulative RTD F(t).

5.6 Refinement of the Parallel Plate Law

Iwai (1976) and Witherspoon et al. (1979) have shown that at low Reynolds numbers, the cubic law [Eq. (38)] is generally valid for flow through fractures. However, the equivalent hydraulic aperture w_h is a weighted average accounting for the distribution of apertures encountered by fluid passing through the fracture. This parameter is probably different from equivalent apertures encountered by tracer, w_t, and thus requires a revision of Eqs. (40) and (41). The reason for the discrepancy is illustrated in the schematic in Figure 30, a rough fracture of varying aperture along the length of the flow path. Because of the w^3 dependence on flow rate, the narrow apertures will contribute the most to the pressure drop. On the other hand, tracer molecules sample the entire flow volume and thus w_t is a straight average of apertures encountered in the flowpath. The tracer aperture w_t will thus always be larger than w_h.

The simplest way to account for roughness is to postulate a distribution of apertures in a rough fracture, calculate the equivalent apertures w_h and w_t, and obtain a relationship between them. Assume a distribution of apertures n(w) such that n(w)dw is the fraction of the flow length with apertures between w and w + dw. Since the order in which fluid encounters different apertures has no effect on the overall pressure drop, we may transform the expression for flow rate to one involving the aperture distribution. Let P(w,w+dw) = the pressure drop through the portion of the fracture with apertures between w and w+dw. Then

$$\Delta P(w,w+dw) = \frac{-12\mu L q n(w)dw}{w^3} \quad . \tag{42}$$

Summing over all apertures,

$$\Delta P = -12\mu L q \int_0^\infty \frac{n(w)dw}{w^3} \tag{43}$$

and the flow rate through the fracture is

$$q = \frac{-\Delta P}{12\mu L \int_0^\infty \frac{n(w)dw}{w^3}} \quad . \tag{44}$$

Comparing Eqs. (44) and (38), we find the equivalent hydraulic aperture w_h is

$$w_h = \left[\int_0^\infty \frac{n(w)dw}{w^3} \right]^{-1/3} \quad . \tag{45}$$

The tracer residence time in the fracture is

$$\tau_c = \frac{L}{q} \int_0^\infty wn(w)dw \quad , \tag{46}$$

resulting in an equivalent tracer aperture w_t given by

$$w_t = \int_0^\infty wn(w)dw \quad . \tag{47}$$

Tsang (1984) and Tsang and Tsang (1987) published data of aperture distributions measured by scanning the faces of a natural granite fracture in a 12-cm core. The results are reproduced in Figure 31. They fit these data to a Gamma distribution and generated random fracture aperture distributions. Our goal is to integrate Eqs. (45) and (47) directly to calculate the ratio of w_h and w_t. Unfortunately, the integral for w_h is infinite for the Gamma distribution, so a different form for n(w) had to be selected. One which provides a reasonable fit to Tsang's data is the lognormal distribution:

$$n(w) = \frac{1}{w\sigma\sqrt{2\pi}} \exp\left\{ -\left(\ln \frac{w}{w_o}\right)^2 / 2\sigma^2 \right] \quad , \tag{48}$$

where w_o is an average aperture and σ is the lognormal standard deviation of apertures. The curve in Figure 31 is a least squares fit of the data to a lognormal distribution. The agreement is adequate, although it underestimates the number of small apertures. This result is acceptable because fluid flow will tend to filter out these small apertures by preferentially flowing to sections of the fracture with larger apertures.

Equations (45) and (47) were numerically integrated for different values of w_o and σ, and the ratio w_t/w_h was found to depend only on σ, the standard deviation in the lognormal distribution. Figure 32 summarizes the results for various σ. For $\sigma = 0.682$ [units of ln(m)] found for the Tsang data, $w_t/w_h = 2.359$.

Finally, expressions involving only w_t can be written for the flow rate and residence time in a fracture. Letting $f_w = w_t/w_h$,

$$q = \frac{-w_t^3 \Delta P}{12\mu L f_w^3} \quad . \tag{49}$$

Notice that this refinement of the parallel plate law does not change the calculation of the pressure field since the f_w's cancel when Eq. (40) is rederived. However, the flow rates are lower by a factor of f_w^3 than if we assume $w_t = w_h$. Accordingly, the residence times within a fracture increase by this factor, so that

$$\tau_c = \frac{12\mu L^2 f_w^3}{w_t^2 \Delta P} \quad . \tag{50}$$

For the Tsang data, this factor is $2.359^3 = 13.13$.

The FRACNET code allows the user to choose the value of f_w. Until better data are available, we will assume $f_w = 2.359$ as determined earlier. Fundamental experimental and theoretical work is needed to validate this model. Cores should be fractured and aperture profiles measured as in the Tsang (1984) study. In addition, simultaneous fluid flow and tracer experiments would allow w_h and w_t to be compared directly without assuming a particular distribution n(w).

5.7 Sample Calculation Using FRACNET

The fracture network generated above will be used to demonstrate the ability of the code to simulate fluid flow and conservative solute transport in a two-well tracer experiment. The properties of the fracture network are given below:

	Fracture Set 1	Fracture Set 2
Number of fractures	200	200
Length (avg. and s.d.)	200, 0 m	100, 0 m
Orientation (avg. and s.d.)	π/2, 0.1	π/3, 0.1
Aperture (avg. and s.d.)	0.4, 0 mm	0.2, 0 mm

The pressure drop from the lower, shorter wellbore to the longer wellbore was 2 mPa. The calculated flow rate for this pressure drop was 1.12×10^{-4} m^3/s per unit depth of reservoir. Figure 33 shows the simulated conservative tracer response for a step change in tracer concentration. This curve is the integral of the residence time histogram and represents the integral of the slug tracer injection. The early response within the first several hours, followed by long tailing caused by long-residence-time flow paths, is characteristic of tracer response for flow between two wellbores in fractured media. This result demonstrates the ability of the fracture network approach to realistically simulate flow and transport for interwell flow through fractured media.

5.8 Future Development of the FRACNET Code

To simulate a wider range of transport problems, modifications to the code are being developed for the fracture flow law, boundary conditions, and tracer transport processes.

Fracture Flow Law: At a high enough Reynolds number, fracture flow can deviate from the laminar-flow cubic law. This is especially true near the wellbore, where flow is converging and diverging. A turbulent flow law can easily be incorporated into the model. Ordinarily, this results in an iterative solution of the nonlinear equation set, whereas for laminar flow the equations are linear. However, since an iterative solution routine is already being employed, the nonlinear problem can be incorporated with very little additional code development.

Boundary Conditions: There need not be only one source and one sink point for the flow system. Usually, more than one fracture intersects the borehole, and often more than two boreholes are present. The code currently handles this situation. Also, boreholes may be present only to sample the fluid without creating a pressure sink. This change will be implemented to simulate hydrologic and tracer studies at the C-wells.

The outer boundaries can also be revised to simulate constant-pressure or constant-flux boundaries, rather than no-flow boundaries. These features will also be implemented.

Tracer Transport Processes: The assumption of a conservative, nonreactive tracer is more restrictive than necessary. The particle-tracking technique can handle any linear transport process (one not dependent on tracer concentration). Adsorption and matrix diffusion will be incorporated into the code by revising the particle-tracking routine.

Chapter 6. Conclusions

1. Reactive tracers with appropriate sorption properties can be used to characterize saturated zone transport properties at the C-wells.

2. Interwell sorbing tracer experiments appear to be preferable to drift-pumpback experiments for characterizing sorption properties.

3. The range of appropriate values of the term a_L in the linear adsorption model is about 0.5 to 3 for interwell experiments and up to 10 for drift-pumpback experiments. If possible, tracers exhibiting linear sorption should be found.

4. Sorption isotherms should be measured over a range of 4 orders of magnitude in concentration starting at the lowest acceptable concentration in a field experiment. Since sorption could be dependent on fracture aperture and thus surface area, the effect of surface area should be examined by varying the particle size in crushed rock experiments. The issues of mineralization on fracture faces should also be addressed.

5. Kinetics effects must also be examined in batch sorption studies. For interwell experiments, kinetics must be studied on the time scale of 0 to 24 h; for drift-pumpback experiments, two time scales are important: 1 to 2 months for the drift phase and 0 to 2 h for the pumpback.

6. The RTD models allow simulations of reactive tracer experiments for any arbitrary conservative tracer response. The maximum mixedness model gives one extreme of behavior for a sorbing tracer with a nonlinear isotherm.

7. Recirculation of produced fluid during an interwell tracer experiment should be avoided because the production of reinjected tracer masks the tail of the response curve.

8. Two numerical codes, TRACR3D and FEHM, will be used to model hydrology, thermal effects, and solute transport for the C-wells, assuming an equivalent porous medium.

9. A new fracture network model, FRACNET, is being developed to model fluid flow and tracer transport in fractured media. Wellbore source and sink boundary conditions are realistically represented. Particle-tracking techniques are used to simulate conservative and reactive tracer transport.

10. The RTD-based models, when revised to include kinetics effects and spatially varying sorption properties, will provide an alternative approach for interpreting interwell reactive tracer experiments in porous media.

NOMENCLATURE

a_L	nondimensional sorption parameter in Langmuir model = $a^* b_1$
a^*	rock surface area to fluid volume ratio (m^2/m^3)
b	nondimensional sorption parameter in Langmuir model = $b_2 C_{ref}$
b_1	parameter in Langmuir adsorption model
b_2	parameter in Langmuir adsorption model
C	nondimensional concentration (C^*/C_{REF})
C^*	concentration of solute (kg/m^3)
C_i	nondimensional concentration at node i
C_{in}	nondimensional inlet concentration
C_{ref}	reference concentration (kg/m^3)
D_e	effective dispersion coefficient (m^2/s)
$f(t)$	residence time distribution (s^{-1})
$F(t)$	cumulative residence time distribution
f_w	ratio of w_t/w_h
h	nondimensional mesh spacing
k	reaction rate constant

K_1	nondimensional rate parameter
K_2	nondimensional rate parameter
K_d	volume sorption equilibrium constant (m^3 fluid/kg rock)
K_f	surface sorption equilibrium constant (m^3 fluid/m^2 rock surface)
K_r	dimensionless kinetic parameter
K_{s1}	rate parameter in Langmuir model
K_{s2}	rate parameter in Langmuir model
L	total flowpath length (m)
m_l	mass of tracer in the liquid phase (kg)
m_p	mass of tracer injected in pulse (kg)
m_r	mass of tracer residing on the rock surface (kg)
N_a	sorptive capacity
$N(\lambda)$	$f(\lambda)/(1-F(\lambda))$
n(w)	aperture distribution function
P	pressure (Pa)
Pe	Peclet number = UL/D_e
P_i	pressure at node i (P_a)
Q	fluid flow rate (m^3/s)
q	fluid flow rate per unit depth (m^2/s)
R(C*)	chemical reaction rate expression
R_i	residual at ith node
S	nondimensional surface concentration
S*	surface concentration of solute (kg/m^2)
S_s^*	maximum surface concentration of solute (kg/m^2)
t	nondimensional time = t^*/τ
t*	time (s)
t_d	drift time (s)
t_p	time for tracer to return during pumpback (s)
U	velocity (m/s)
U_d	drift-phase velocity (m/s)
U_p	pumpback flow velocity (m/s)
V_l	liquid volume (m^3)
w	fracture aperture (m)
w_h	equivalent hydraulic aperture (m)
w_o	aperture in lognormal distribution (m)
w_t	equivalent tracer aperture (m)

w_r	mass of rock (kg)
x	nondimensional flowpath distance = x^*/L
x^*	distance along the flowpath (m)
X	distance travelled by tracer during drift (m)
β	Crank-Nicholson parameter
ϕ	porosity
δ^j	correction $C^{j-1} - C^j$ in Newton's method
λ	life expectation of a molecule in a flow system (s)
μ	fluid viscosity (Pa-s)
ρ_b	bulk rock density (kg/m^3)
τ	mean residence time of fluid = L/U (s)
τ_c	conservative tracer transport time (s)
τ_f	characteristic fluid residence time (s)
τ_r	characteristic adsorption reaction time (s)

REFERENCES

Andersson, J., and R. Thunvik, "Predicting Mass Transport in Discrete Fracture Networks With the Aid of Geometrical Field Data," Water Resour. Res. 22, 13, 1941-1950 (1986).

Brenner, H., "The Diffusional Model of Longitudinal Mixing in Beds of Finite Length, Numerical Values," Chem. Eng. Sci. 17, 229-243 (1962).

Castillo, E., Karadi, G. M., and R. J. Krizek, "Unconfined Flow Through Jointed Rock," Water Res. Bull. 8, 2, 266-281 (1972).

Danckwerts, P. V., "The Effect of Incomplete Mixing on Homogeneous Reactions," Chem. Eng. Sci. 8, 93-102 (1958).

Finlayson, B. A., Nonlinear Analysis in Chemical Engineering (McGraw-Hill Book Co., NY, 1980).

Hopkirk, R. J., Gilby, D. J, Ryback, L., and J. C. Griesser, "Modelling of Heat and Mass Transfer in Deep, Fractured Crystalline Rock," Geothermics 14, 2, 385-392 (1985).

Iwai, K., "Fundamental Studies of Fluid Flow Through a Single Fracture," PhD Dissertation, U. of Calif., Berkeley (1976).

Karasaki, K., "Well Test Analysis in Fractured Media," PhD Dissertation, U. of California, Berkeley (1986).

Long, J. C. S., Remer, J. S., Wilson, C. R., and P. A. Witherspoon, "Porous Media Equivalents for Networks of Discontinuous Fractures," Water Resour. Res. 18, 3, 645-658 (1982).

Robinson, B. A., Aguilar, R. G., Kanaori, Y., Trujillo, P. E., Counce, D. A., Birdsell, S. A., and I. Matsunaga, "Geochemistry and Tracer Behavior During a Thirty Day Flow Test of the Fenton Hill HDR Reservoir," 12th Workshop on Geothermal Reservoir Engineering, Stanford U., Stanford, CA, January 20-22, 1987.

Robinson, B. A., and J. W. Tester, "Dispersed Fluid Flow in Fractured Reservoirs: An Analysis of Tracer-Determined Residence Time Distributions," J. Geophys. Res. 89, B12, 10374-10384 (1984).

Satter, A., Shum, Y. M., Adams, W. T., and L. A. Davis, "Chemical Transport in Porous Media With Dispersion and Rate-Controlled Adsorption," SPEJ, 129-138, June (1980).

Schwartz, F. W., "Macroscopic Dispersion in Porous Media: The Controlling Factors," Water Resour. Res. 13, 4, 743-752 (1977).

Schwartz, F. W., Smith, L., and A. S. Crowe, "A Stochastic Analysis of Macroscopic Dispersion in Fractured Media," Water Resour. Res. 19, 5, 1253-1265 (1983).

Smith, L., and F. W. Schwartz, "Mass Transport 1. A Stochastic Analysis of Macroscopic Dispersion," Water Resour. Res. 16, 2, 303-313 (1980).

Snow, D. T., "The Frequency and Apertures of Fractures in Rock," Int. J. Rock. Mech. Min. Sci. 7, 23-40 (1970).

Travis, B. J., "TRACR3D: A Model of Flow and Transport in Porous/Fractured Media," Los Alamos National Laboratory report LA-9667-MS (1984).

Tsang, Y. W., "The Effect of Tortuosity on Fluid Flow Through a Single Fracture," Water Resour. Res. 20, 9, 1209-1215 (1984).

Tsang, Y.W., and C. F. Tsang, "Channel Model of Flow Through Fractured Media," Water Resour. Res. 23, 3, 467-479 (1987).

Witherspoon, P. A., Wang, J. C. Y., Iwai, K., and J. E. Gale, "Validity of the Cubic Law for Fluid Flow in a Deformable Rock Fracture," Water Resour. Res. 16, 6, 1016-1024 (1979).

Zwietering, T. N., "The Degree of Mixing in Continuous Flow Systems," Chem. Eng. Sci. 11, 1-15 (1959).

Zyvoloski, G., "Finite Element Methods for Geothermal Reservoir Simulation," Int. J. Numer. Anal. Meth. in Geomech. 7, 75-86 (1983).

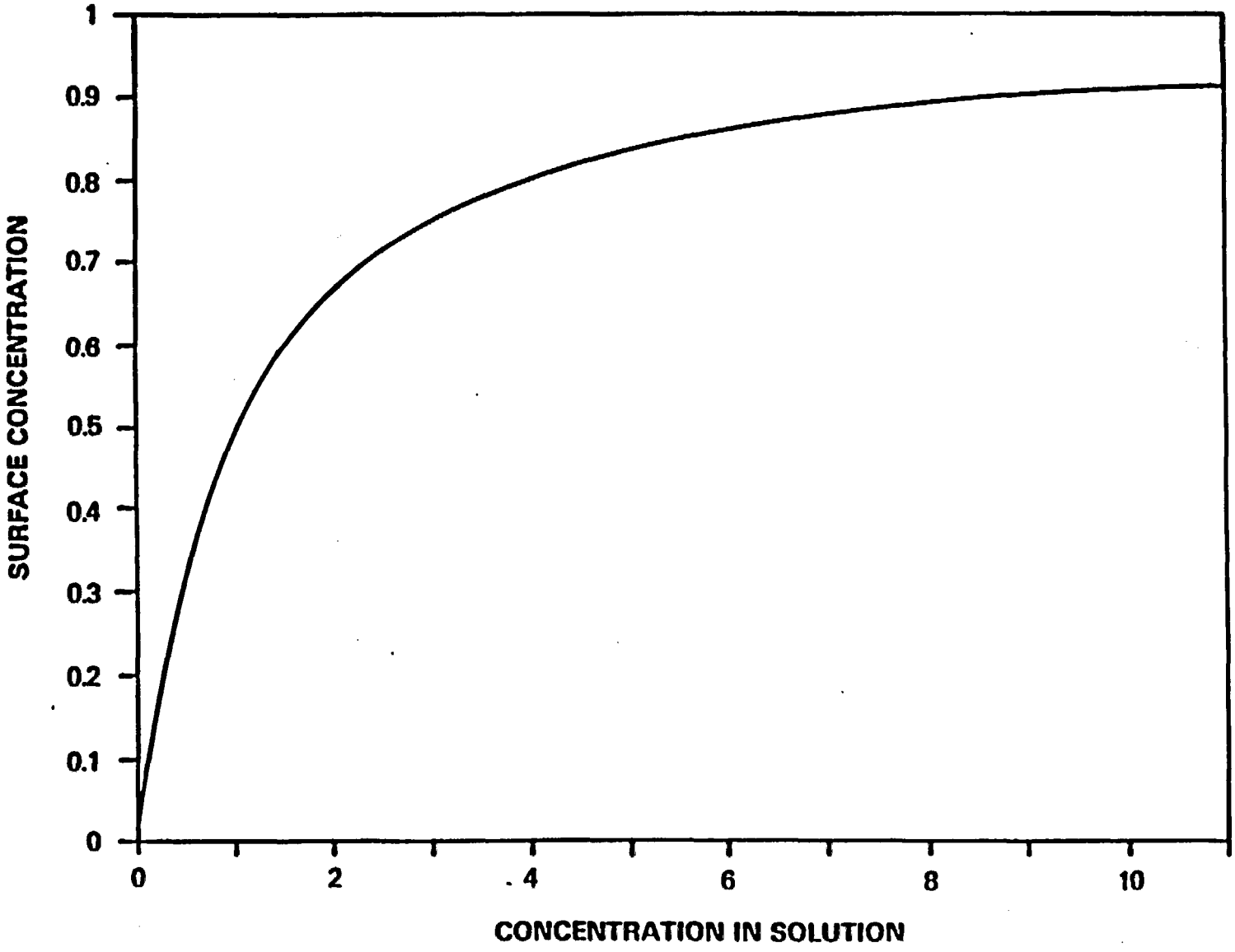

Figure 1. Langmuir adsorption isotherm. b_1=1, b_2=1.

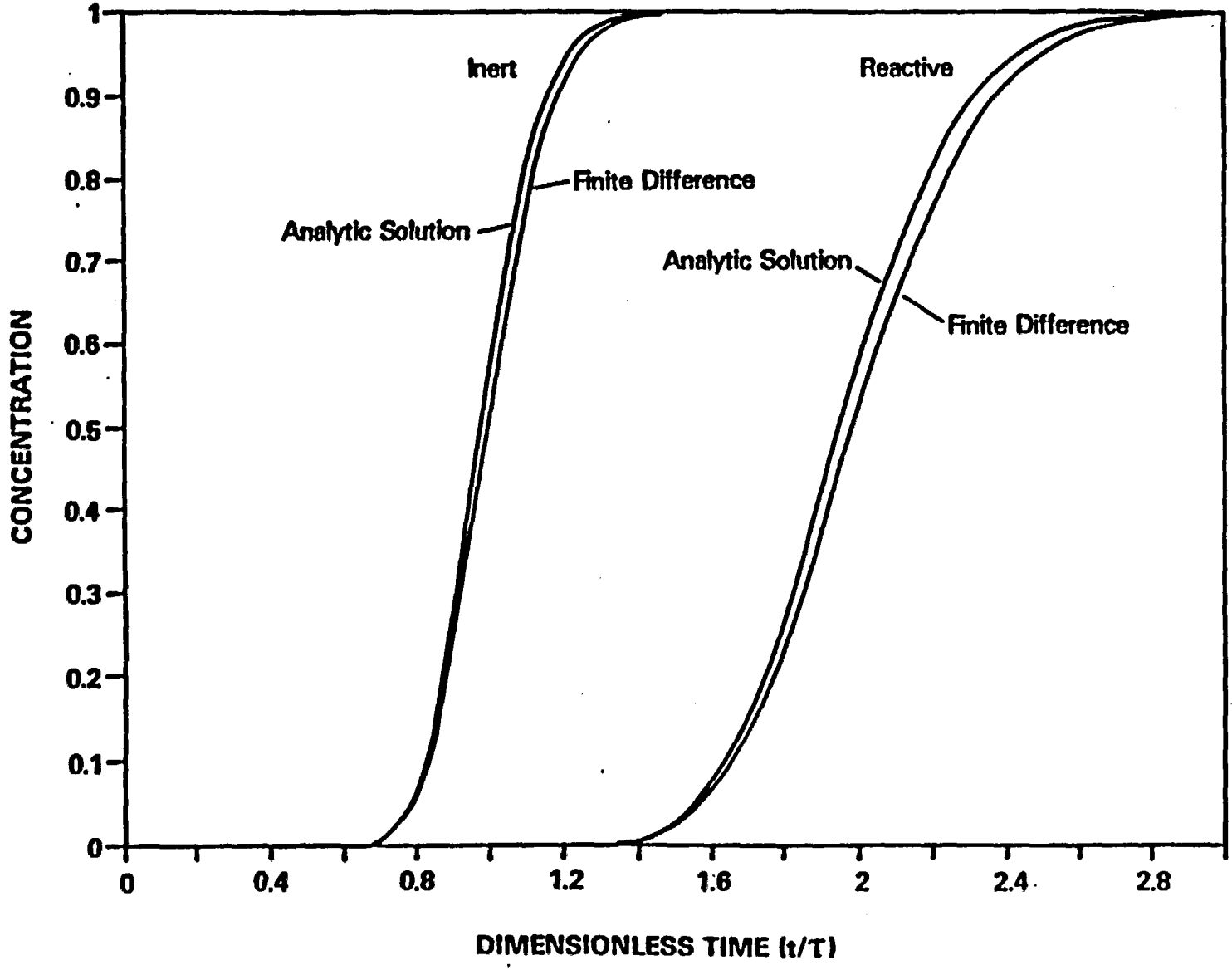

Figure 2. Comparison of finite difference results with an analytic solution for conservative and adsorbing tracers (a_L = 1).

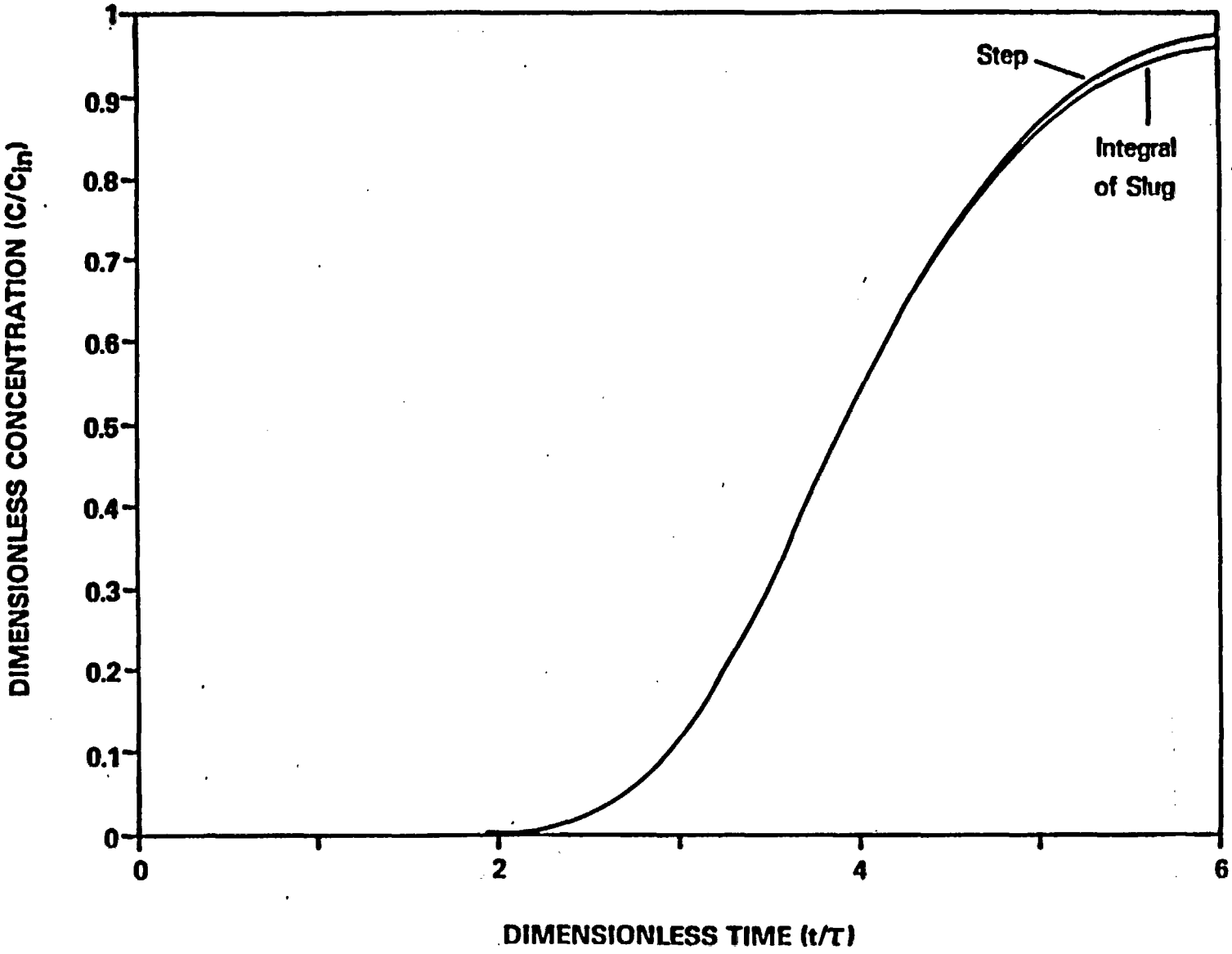

Figure 3. Comparison of step response with integral of the slug injection response for $a_L \approx 3$.

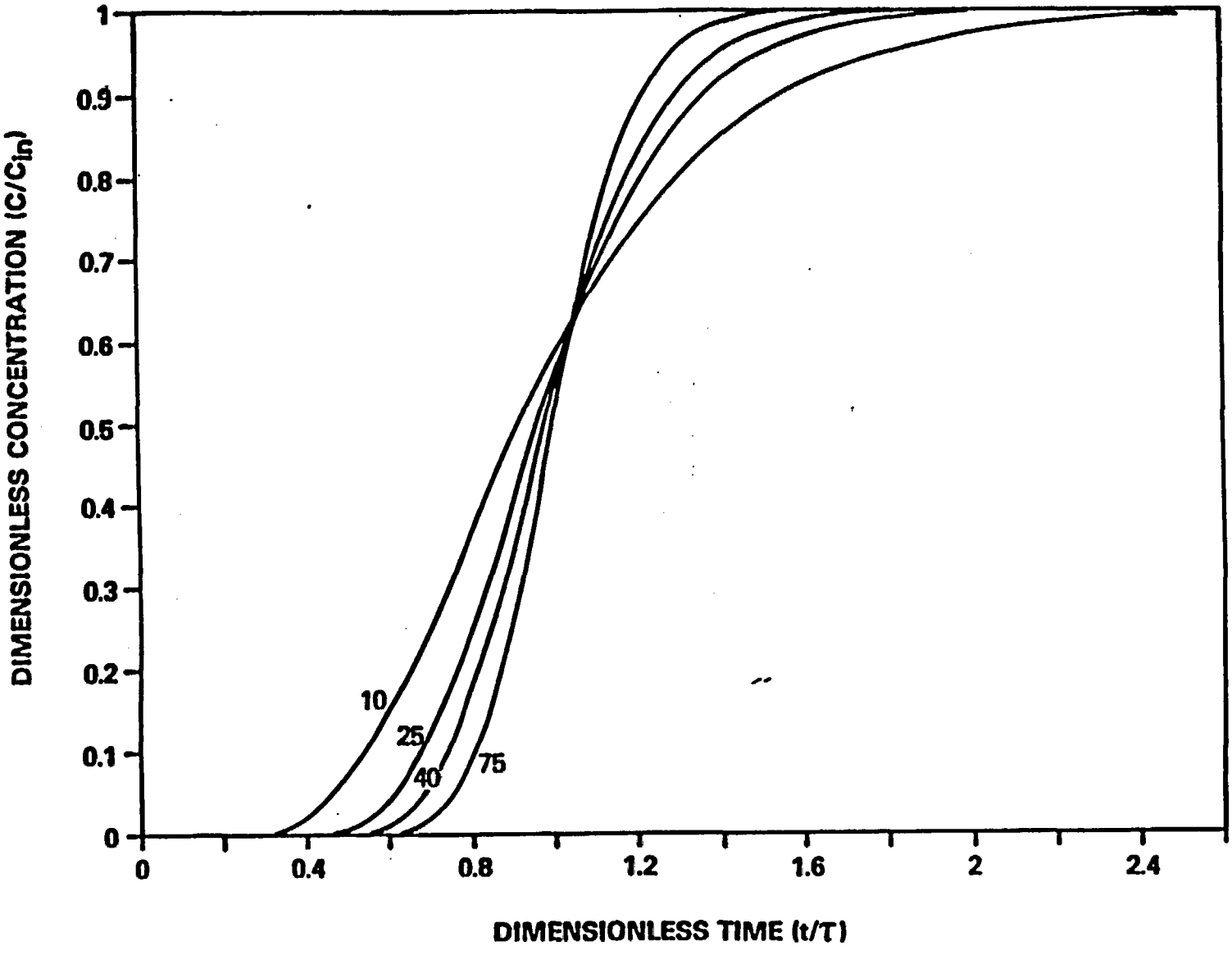

Figure 4. Conservative tracer step responses for different values of the Peclet number.

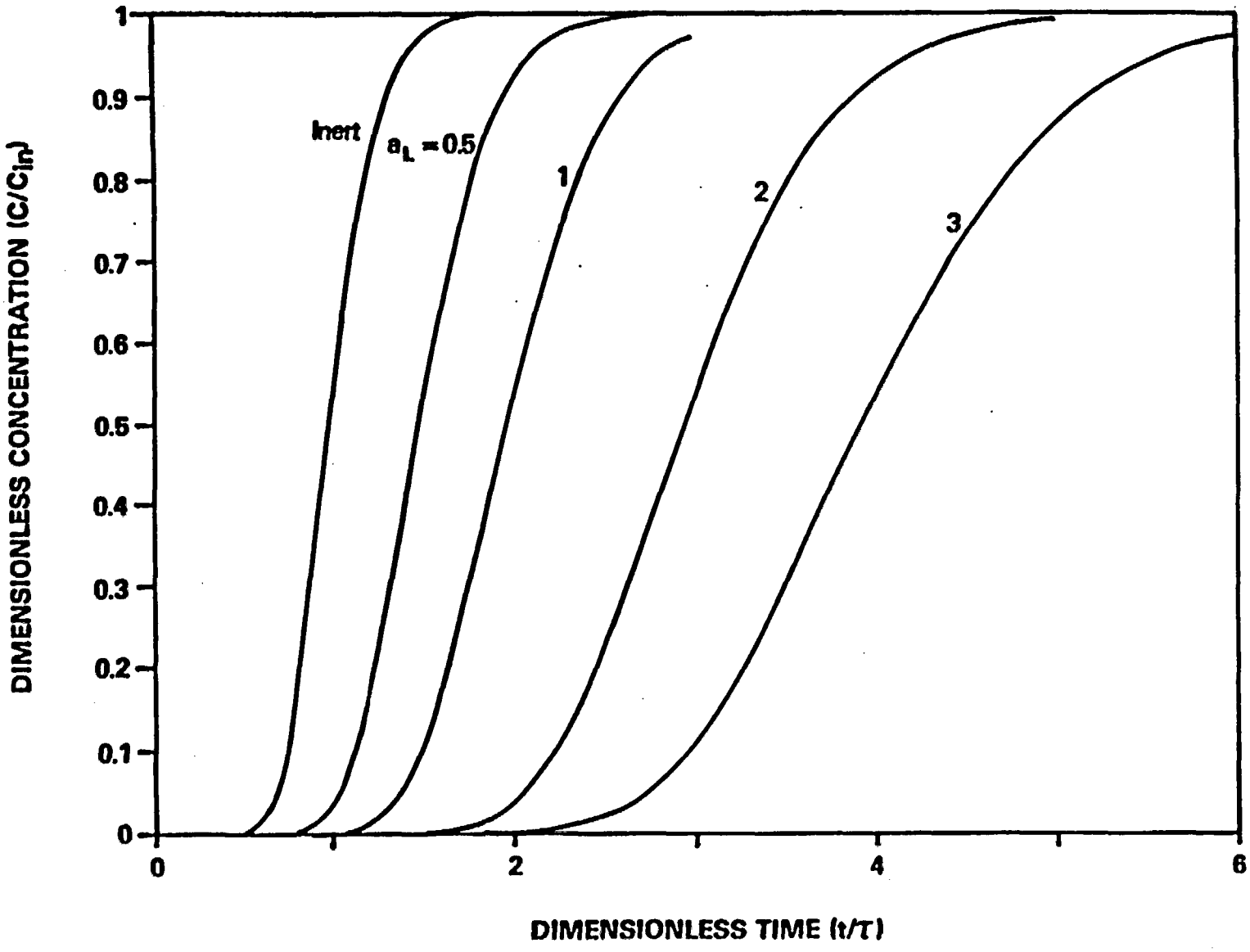

Figure 5. Sorbing tracer step responses for different values of a_L (b=0).

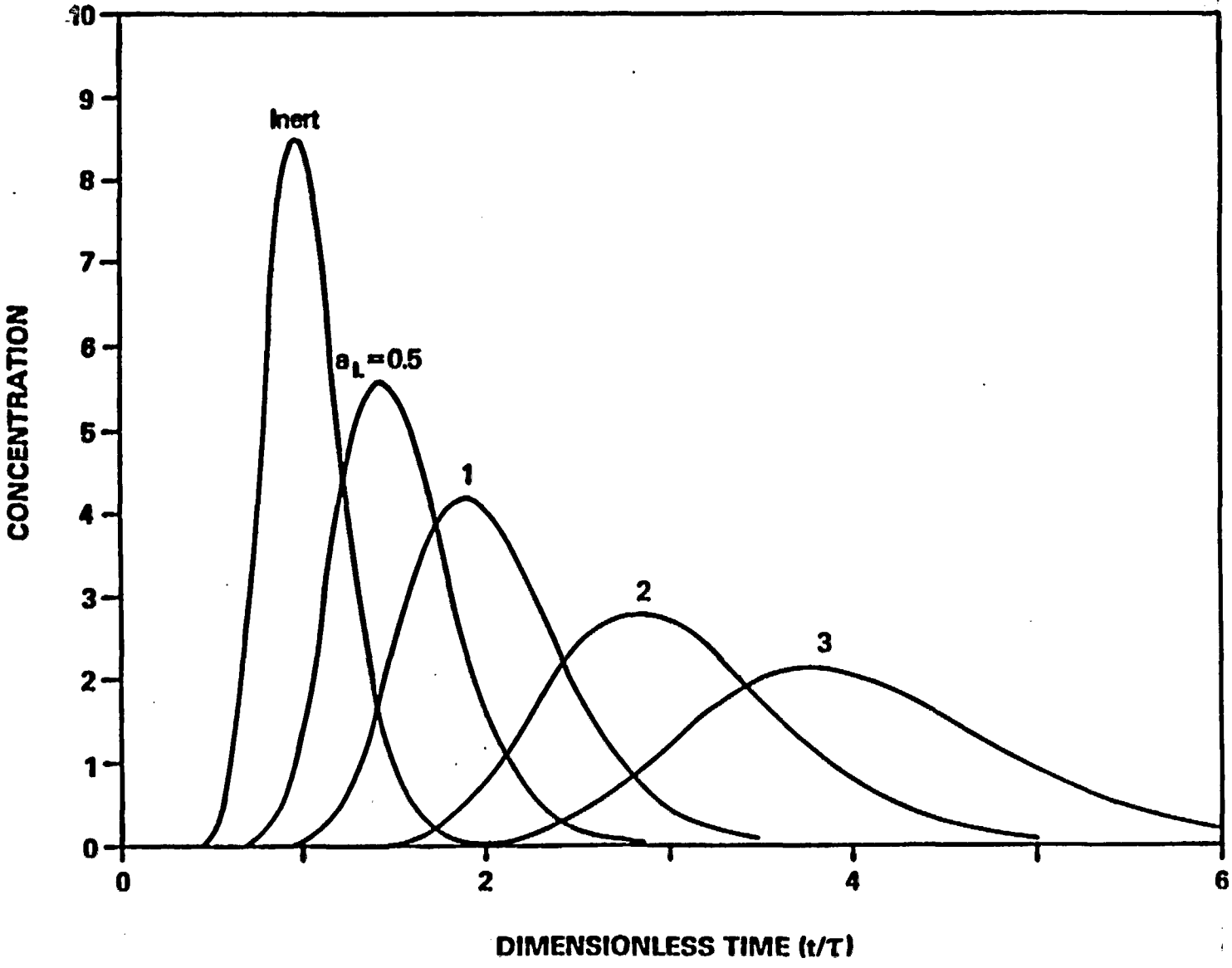

Figure 6. Sorbing tracer slug injection responses for firrerent values of a_L (b=0).

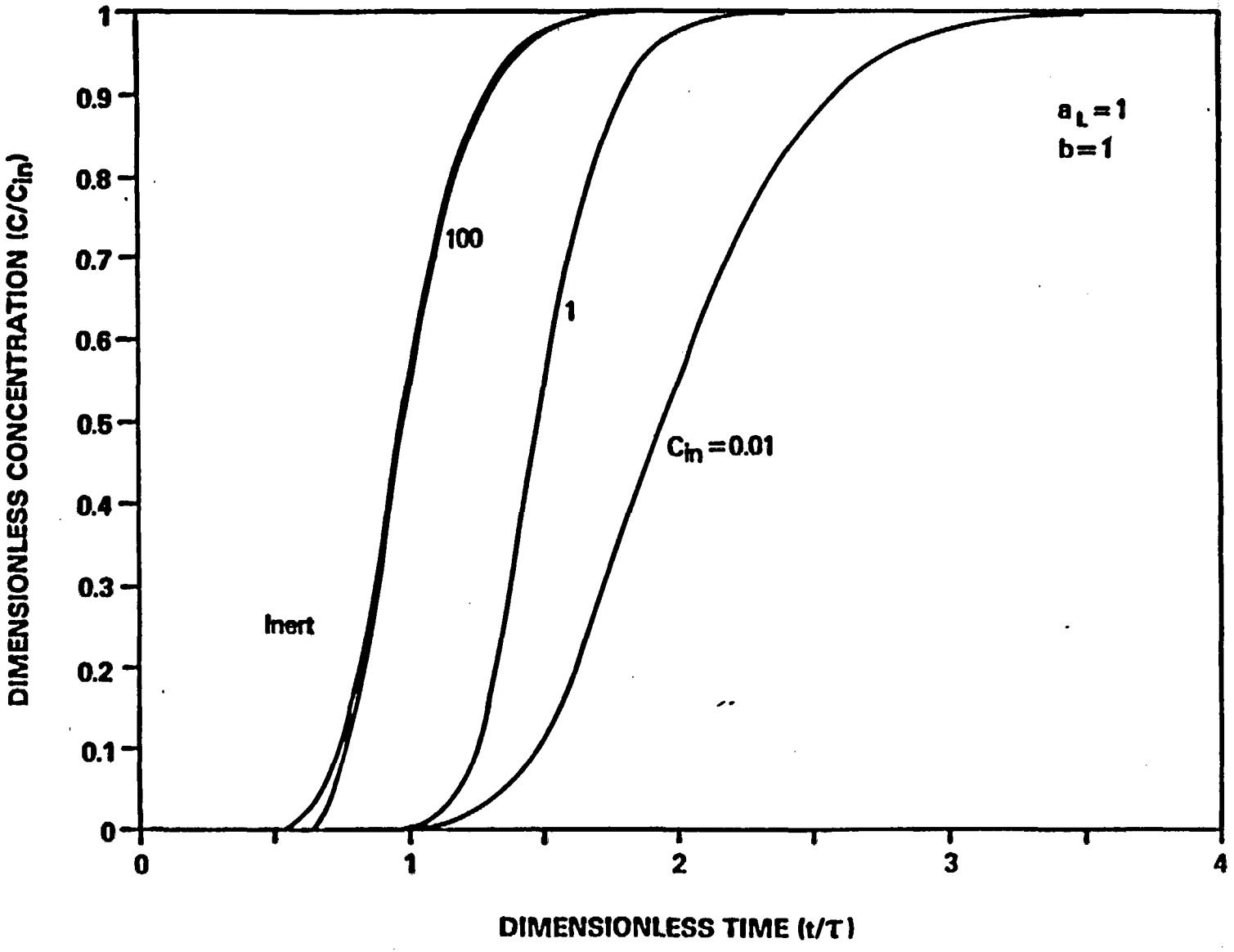

Figure 7. Sorbing tracer step responses for nonlinear adsorption for various values of injection concentration C_{in}.

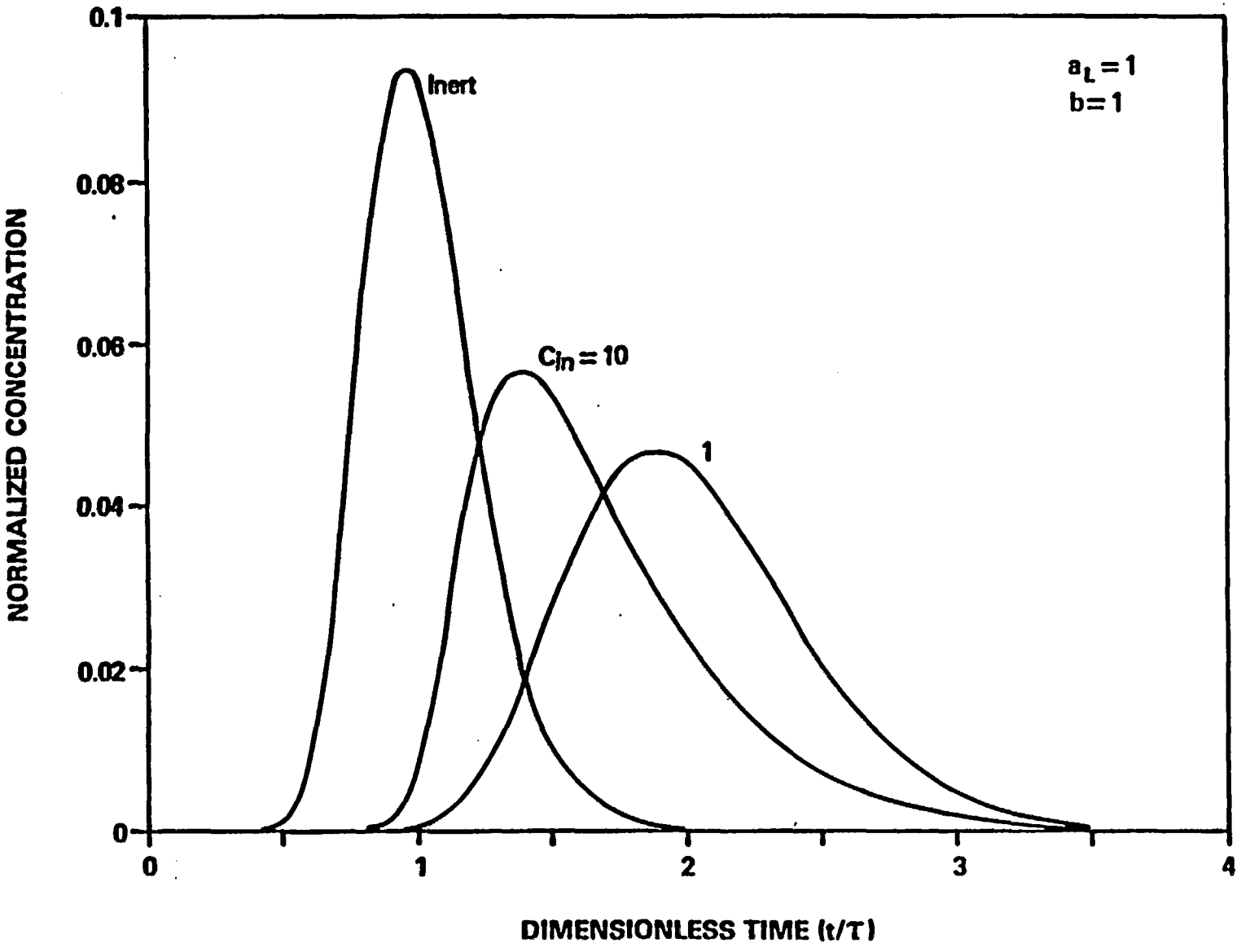

Figure 8. Sorbing tracer slug responses for nonlinear sorption for various values of injection concentration C_{in}. Slug duration is the same for each case.

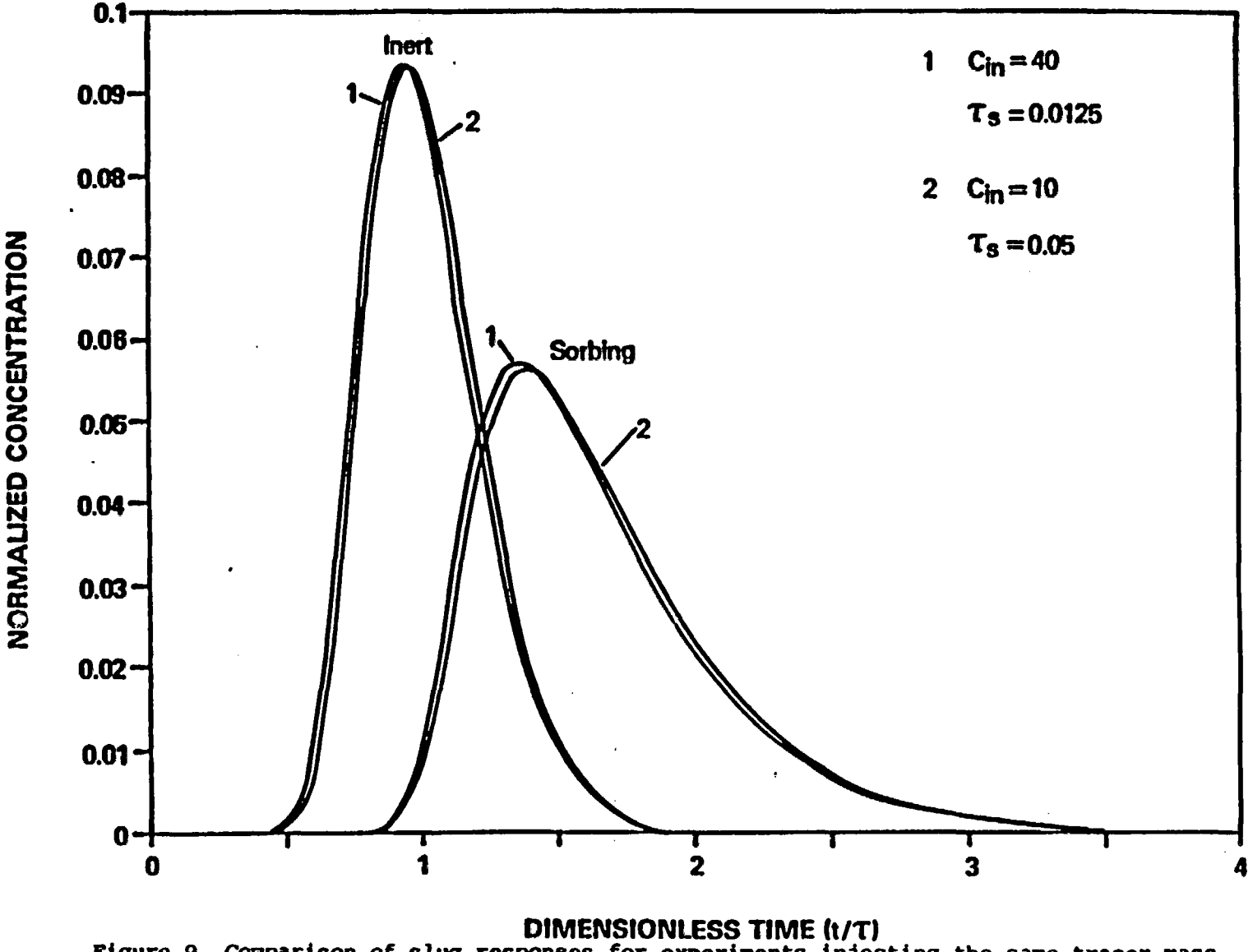

Figure 9. Comparison of slug responses for experiments injecting the same tracer mass but different concentration and slug duration. For the adsorbing tracer case, a_L = 1 and b = 1.

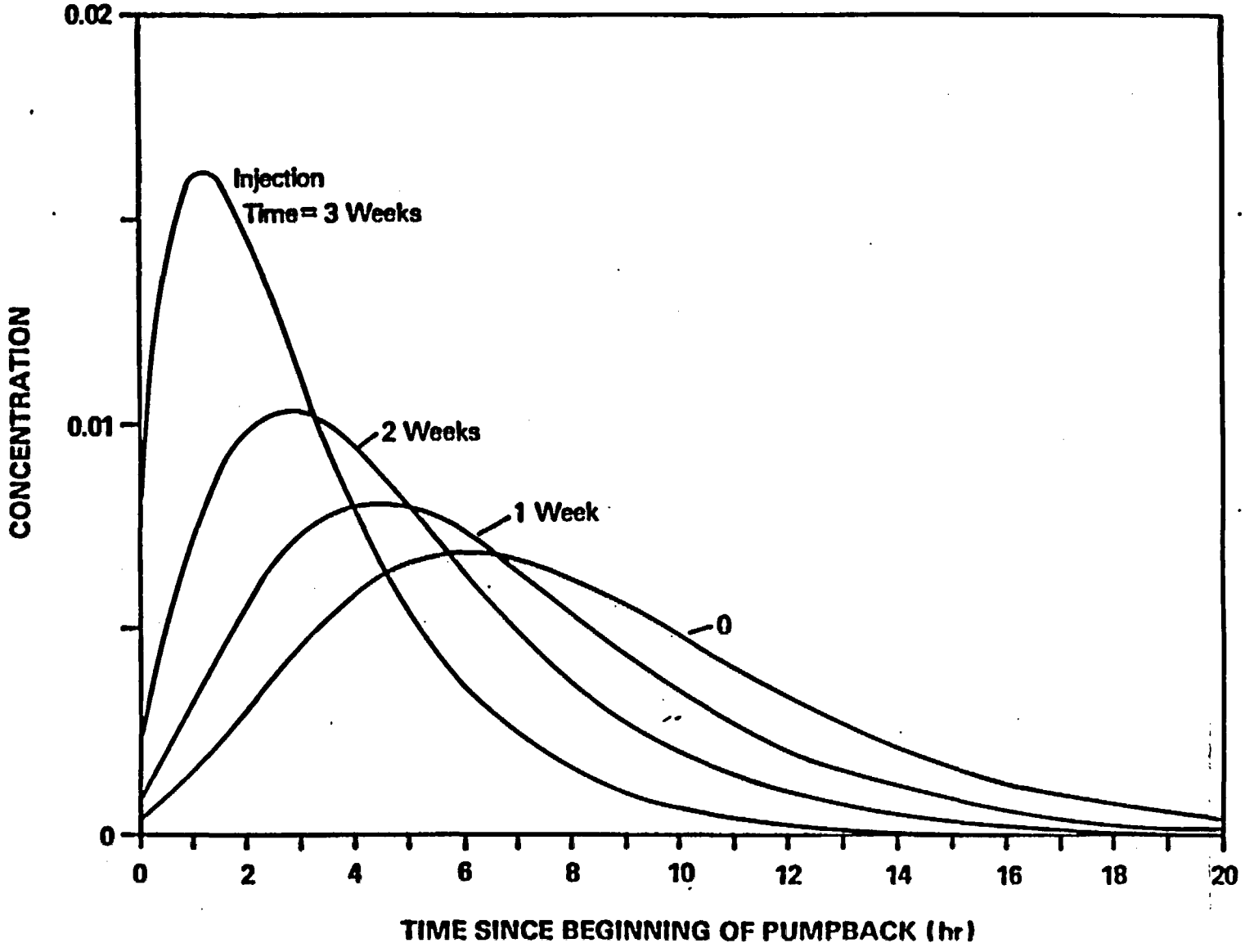

Figure 10. Drift-Pumpback conservative tracer responses for tracers injected at different times during the drift phase.

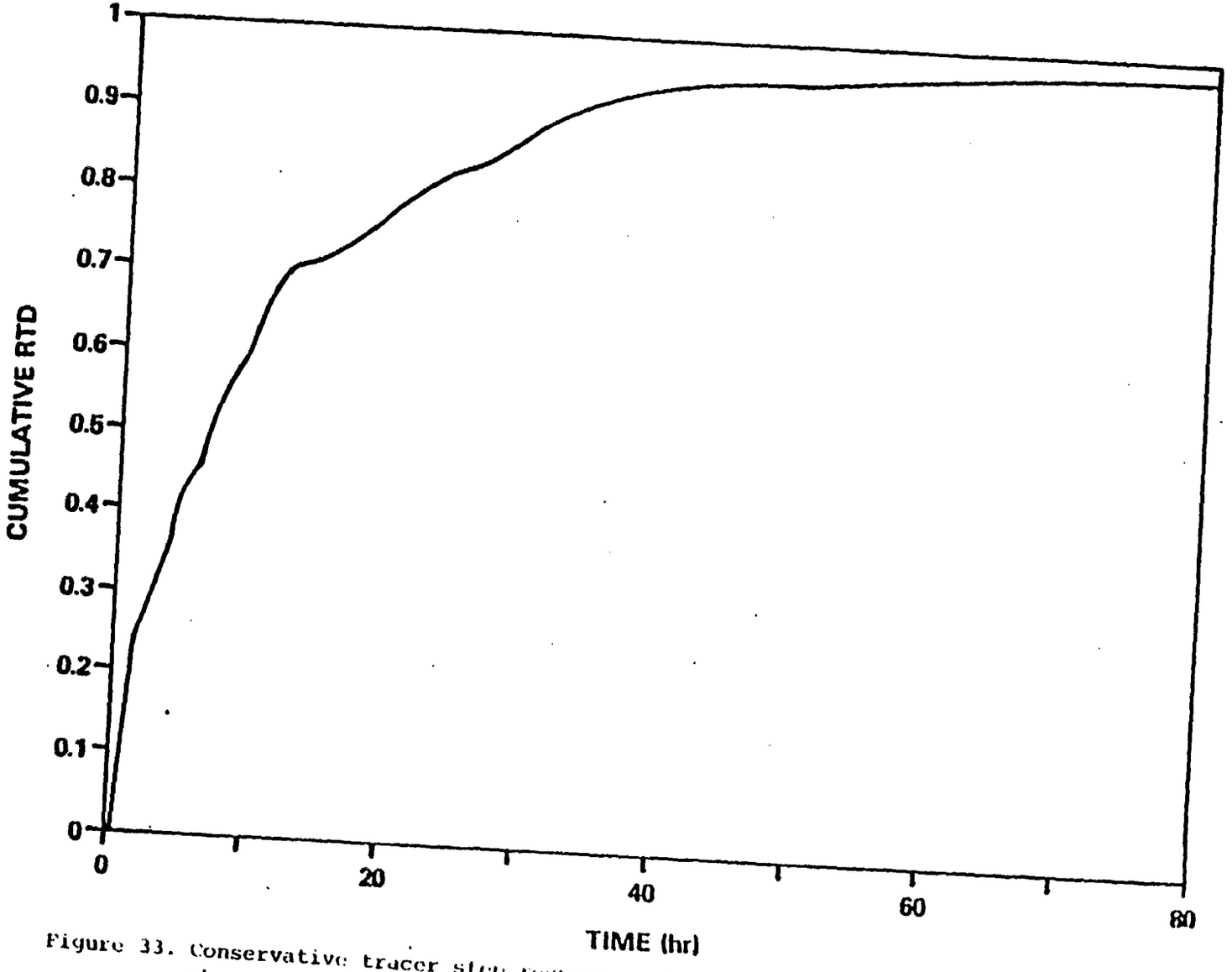

Figure 33. Conservative tracer step response calculated using PRACHET for the network shown earlier

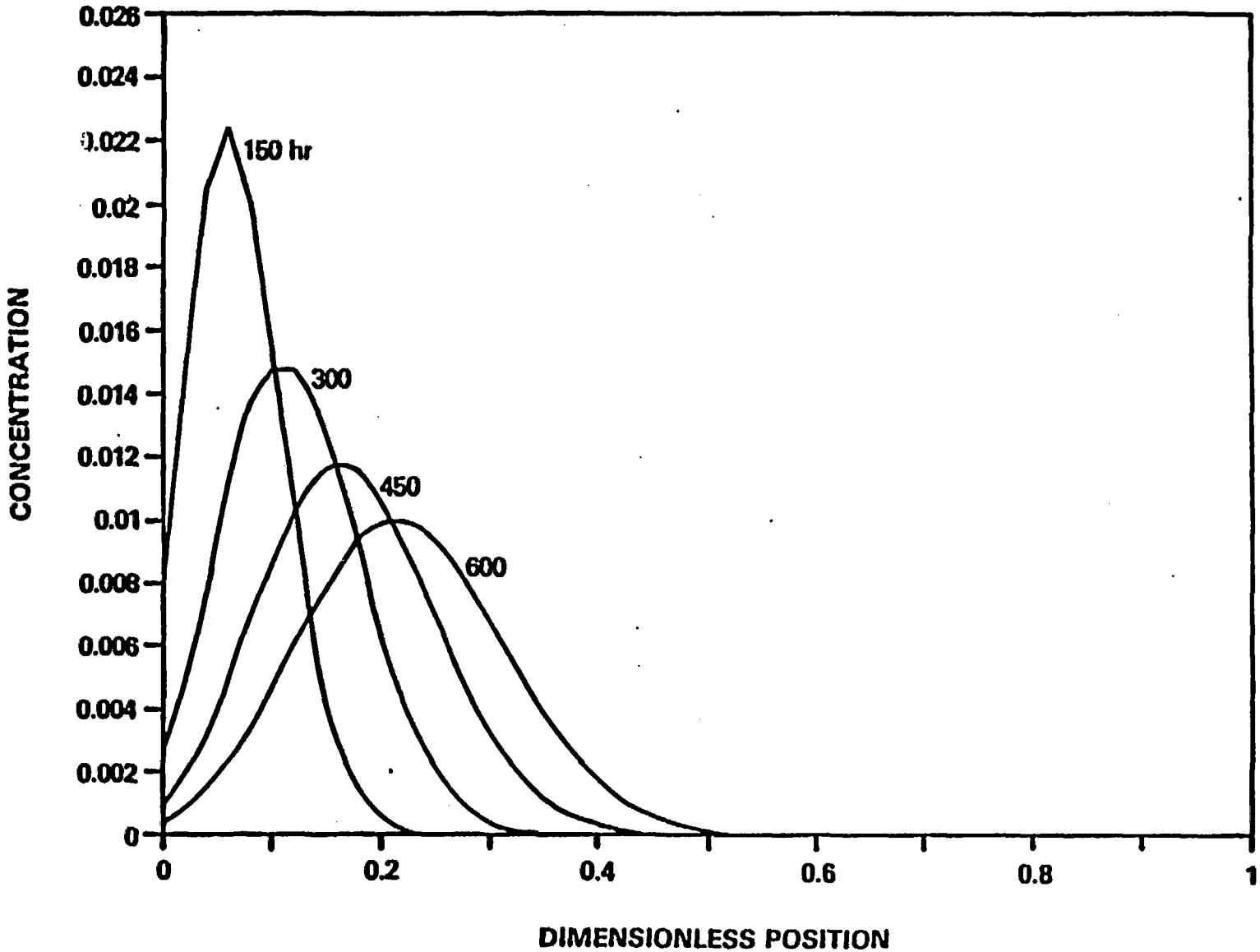

Figure 11. Internal concentration profiles at different times during the drift phase of a drift-pumpback experiment.

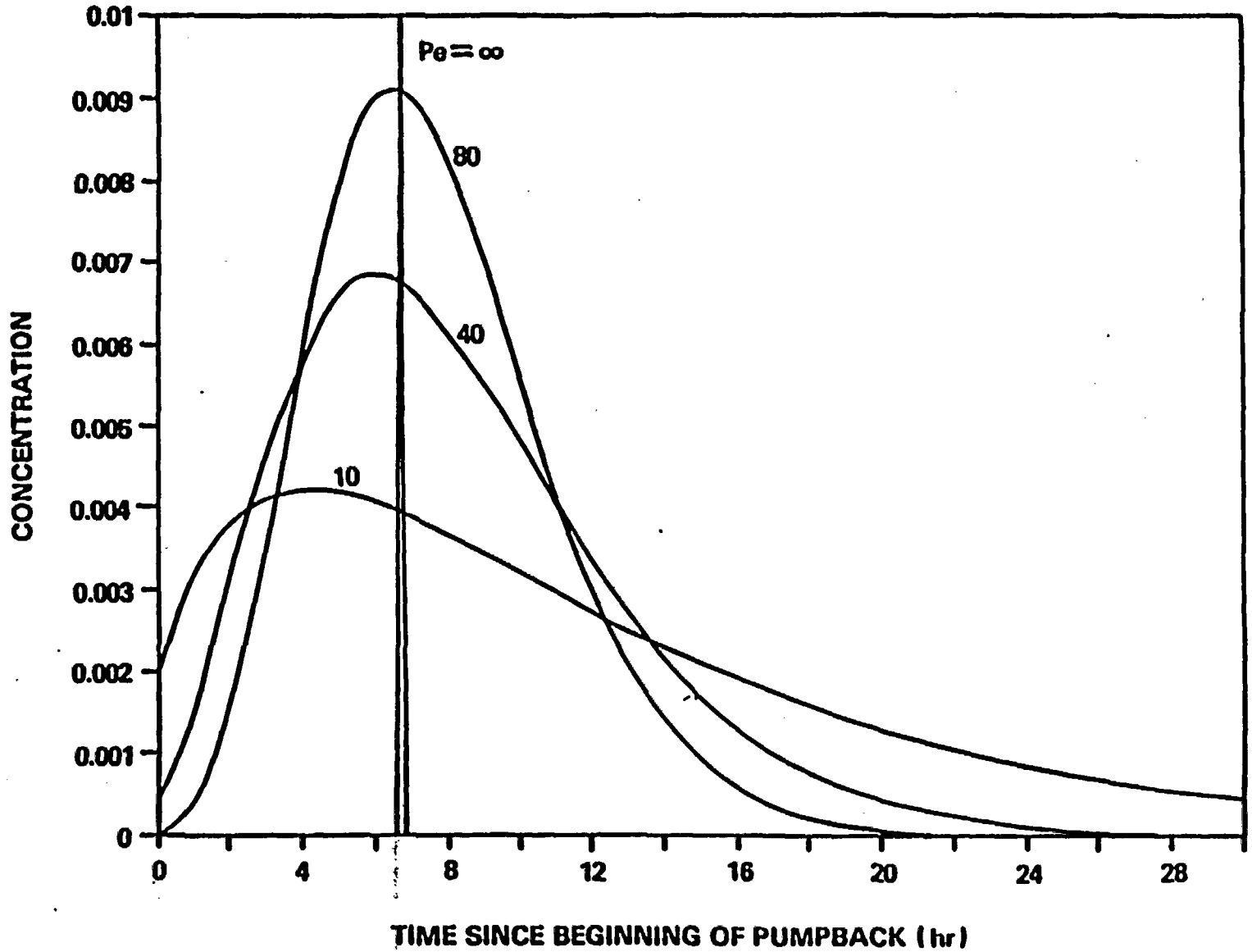

Figure 12. Drift-pumpback conservative tracer responses for different values of the Peclet number.

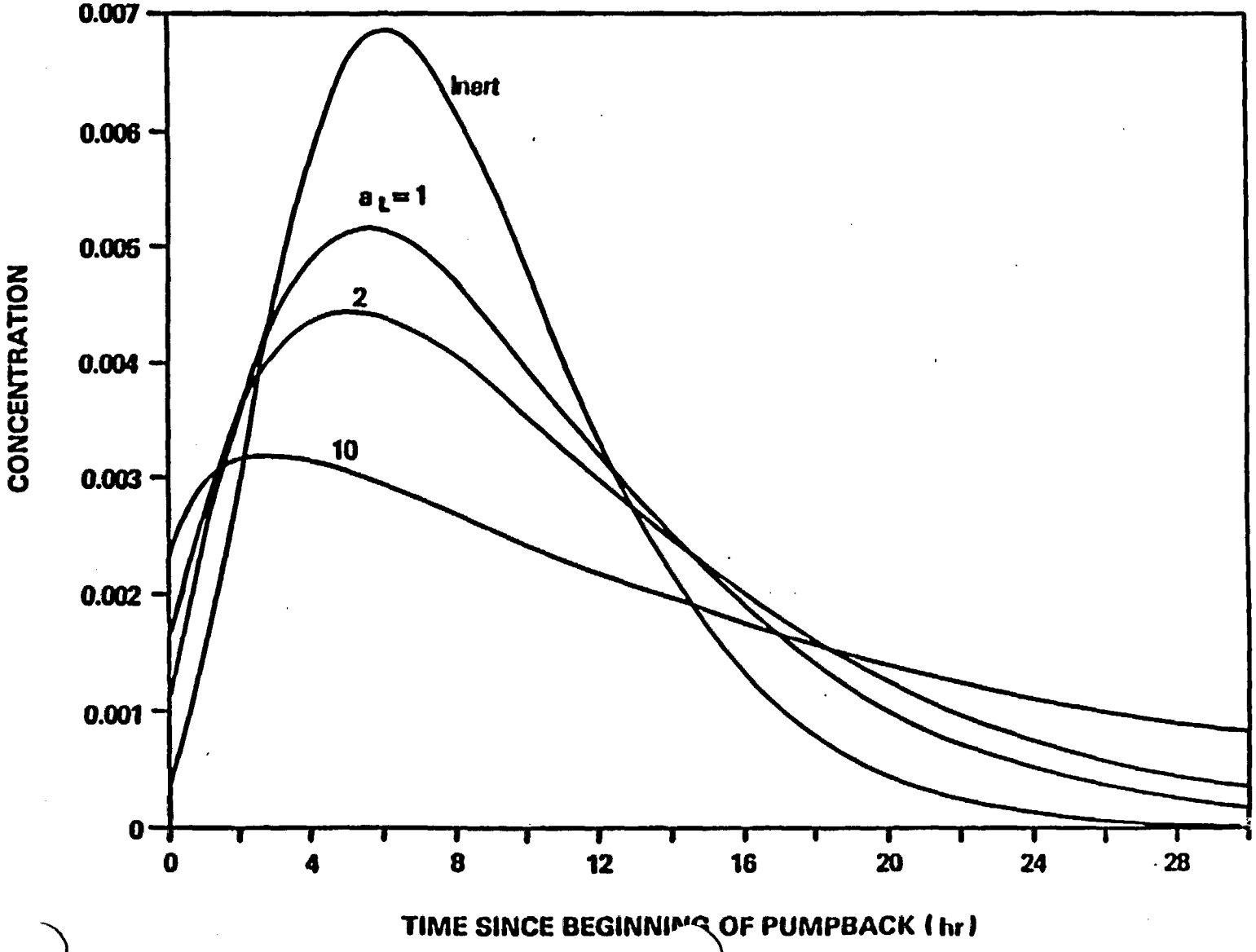

Figure 13. Drift-pumpback sorbing tracer responses for different values of a_L (b=0).

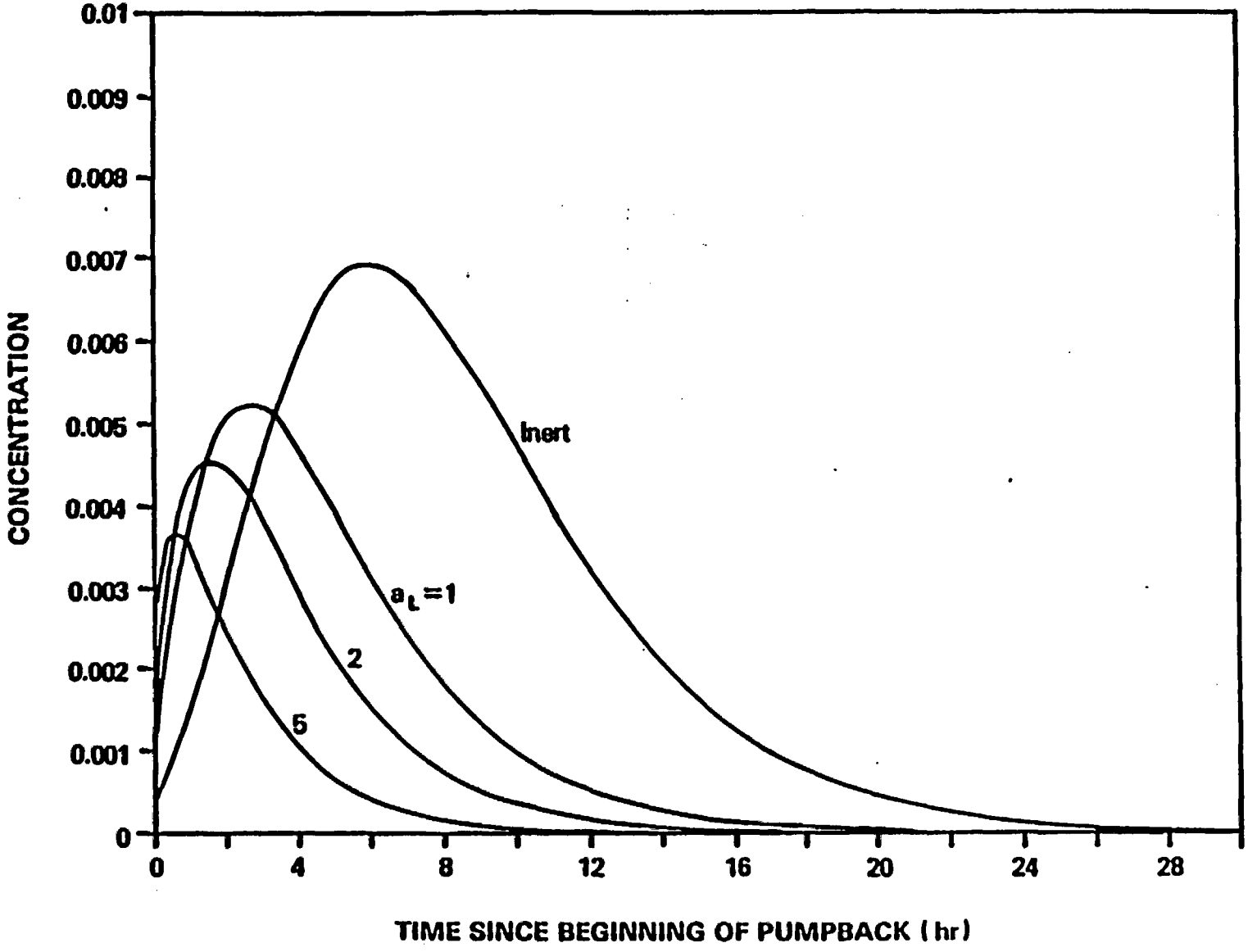

Figure 14. Drift-pumpback sorbing tracer responses for various values of a_L (b=0) assuming adsorption during the drift phase only.

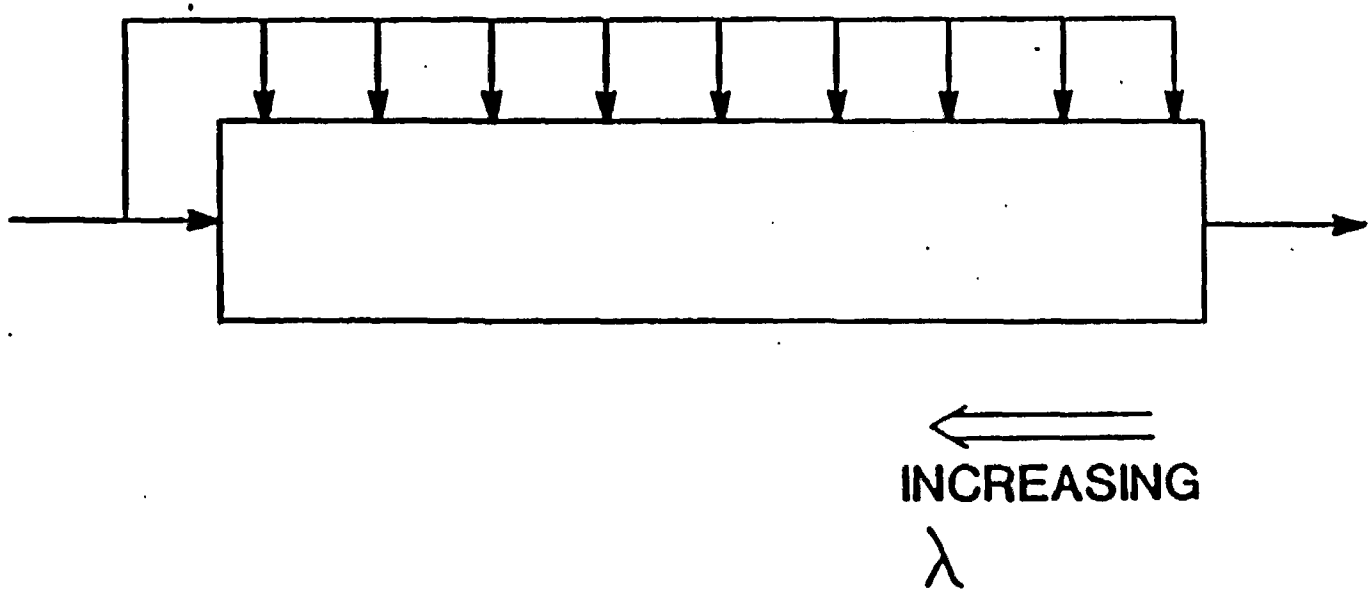

Figure 15. Schematic of the maximum mixedness model of a plug flow reactor with side entrances.

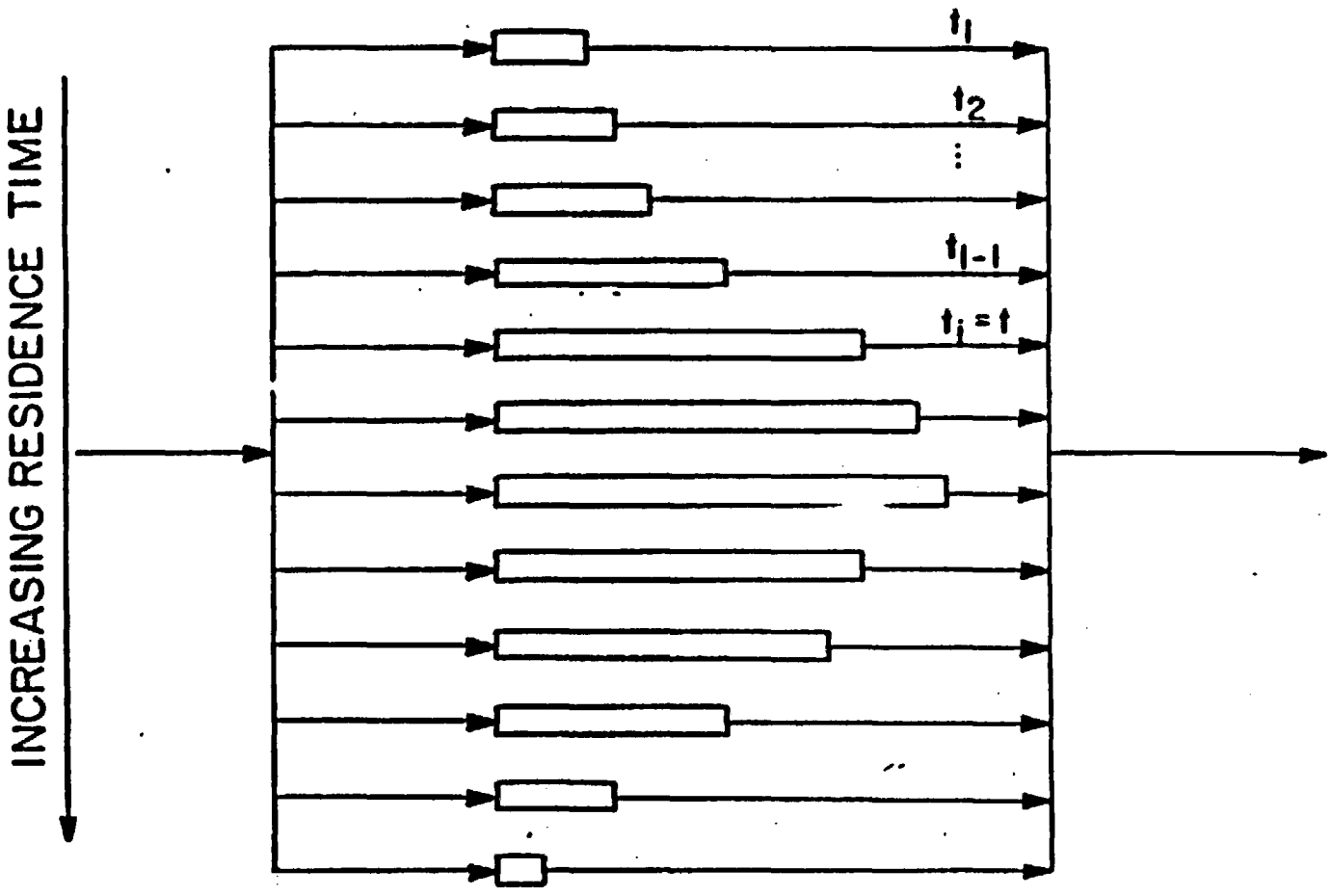

Figure 16. Schematic of the minimum mixedness model of parallel plug flow paths

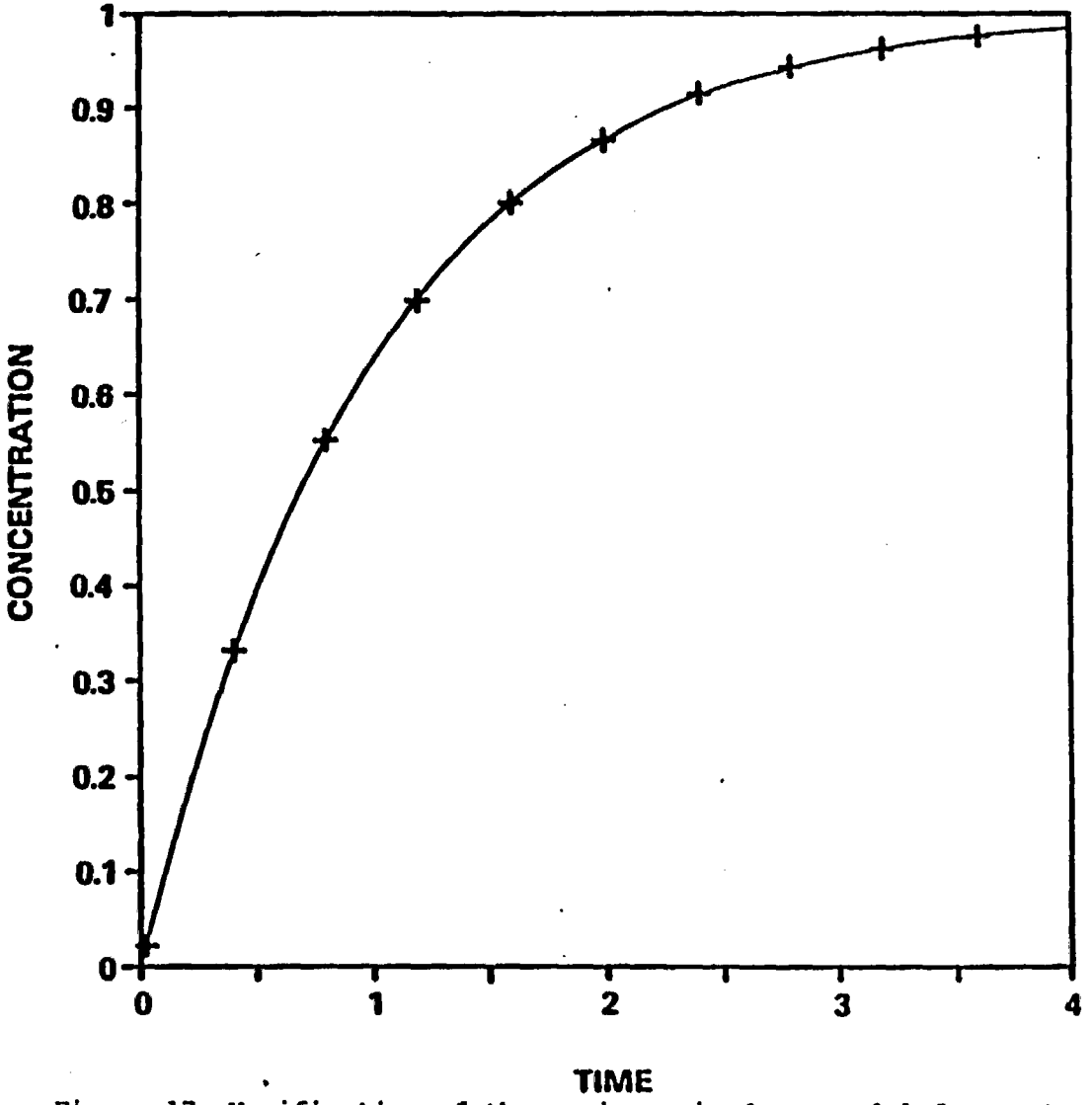

Figure 17. Verification of the maximum mixedness model for a step response of a conservative tracer in a CSTR. The curve is the model, and the +'s are the analytical solution.

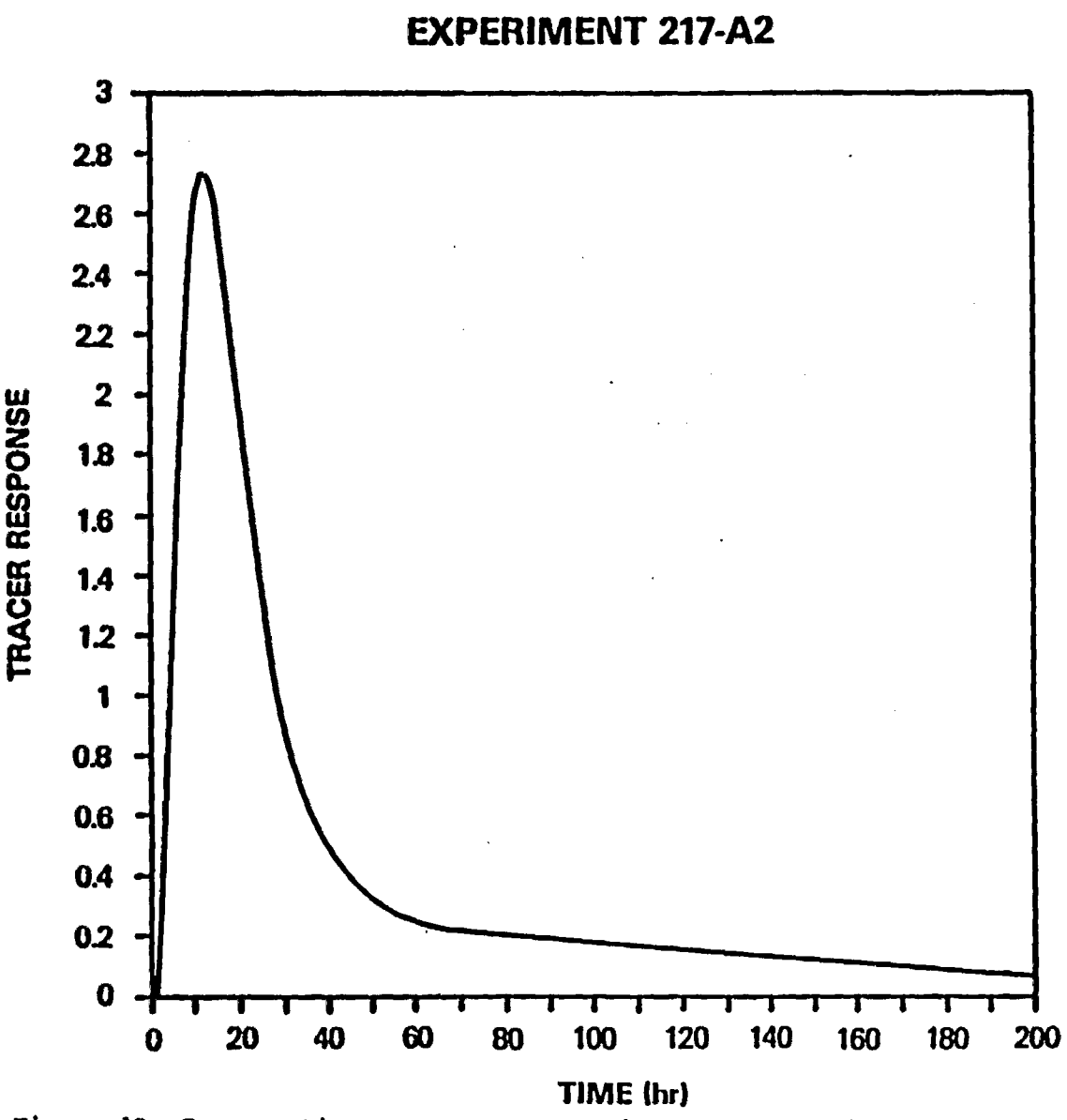

Figure 19. Conservative tracer response in the Fenton Hill, NM Phase I Hot Dry Rock geothermal reservoir (Experiment 217-A2).

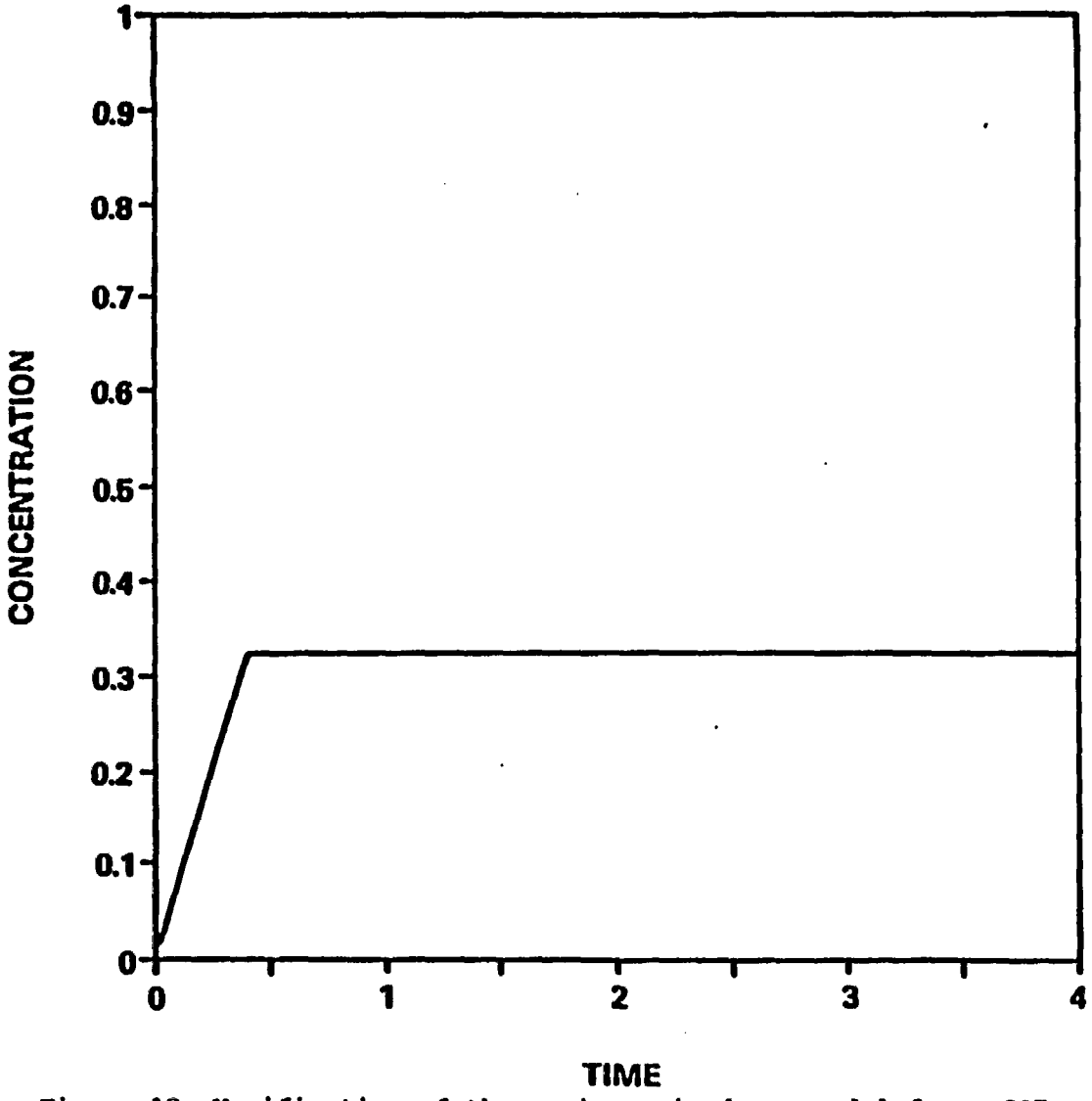

Figure 18. Verification of the maximum mixedness model for a CSTR with recirculation.

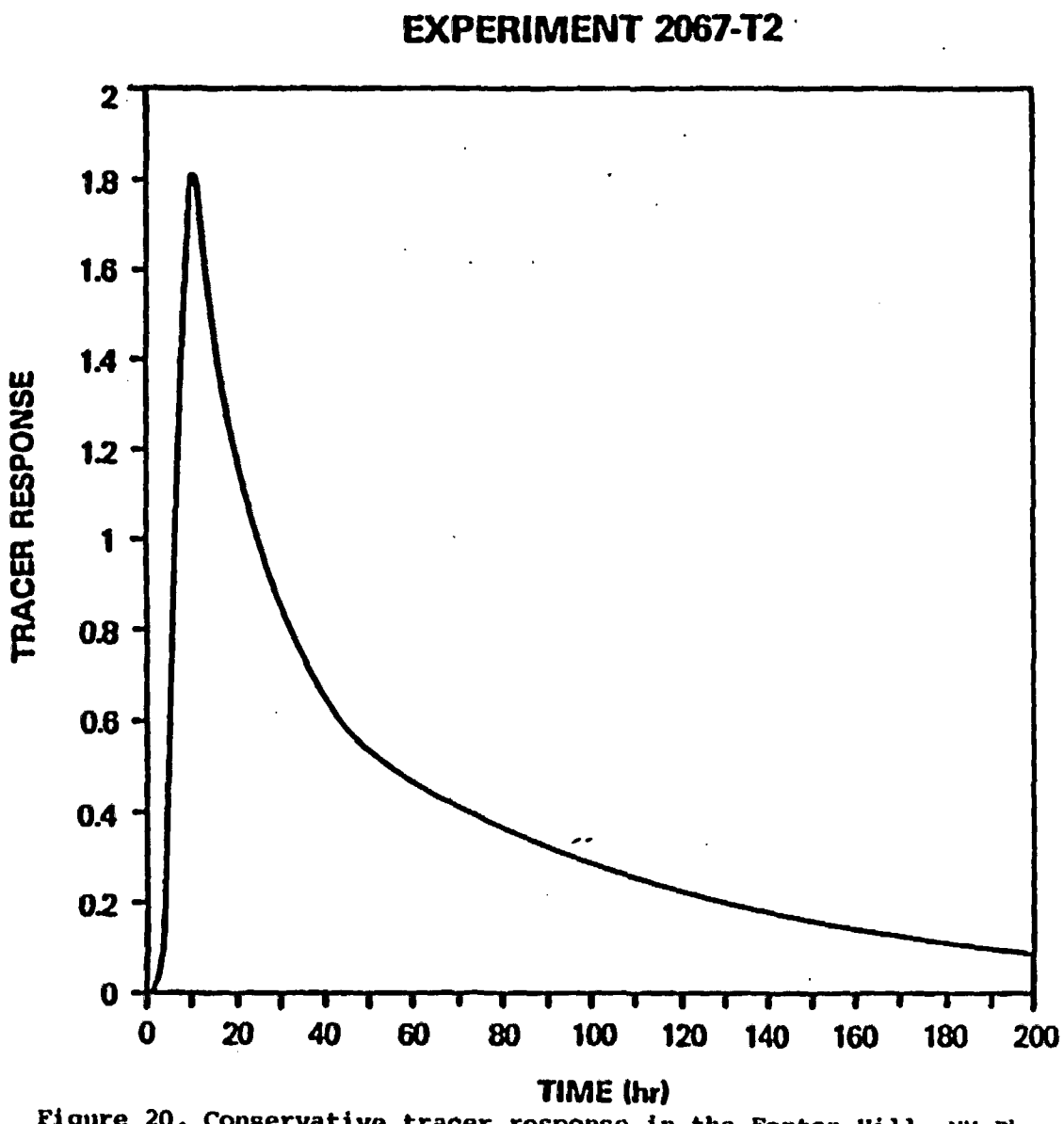

Figure 20. Conservative tracer response in the Fenton Hill, NM Phase II Hot Dry Rock geothermal reservoir (Experiment 2067-T2).

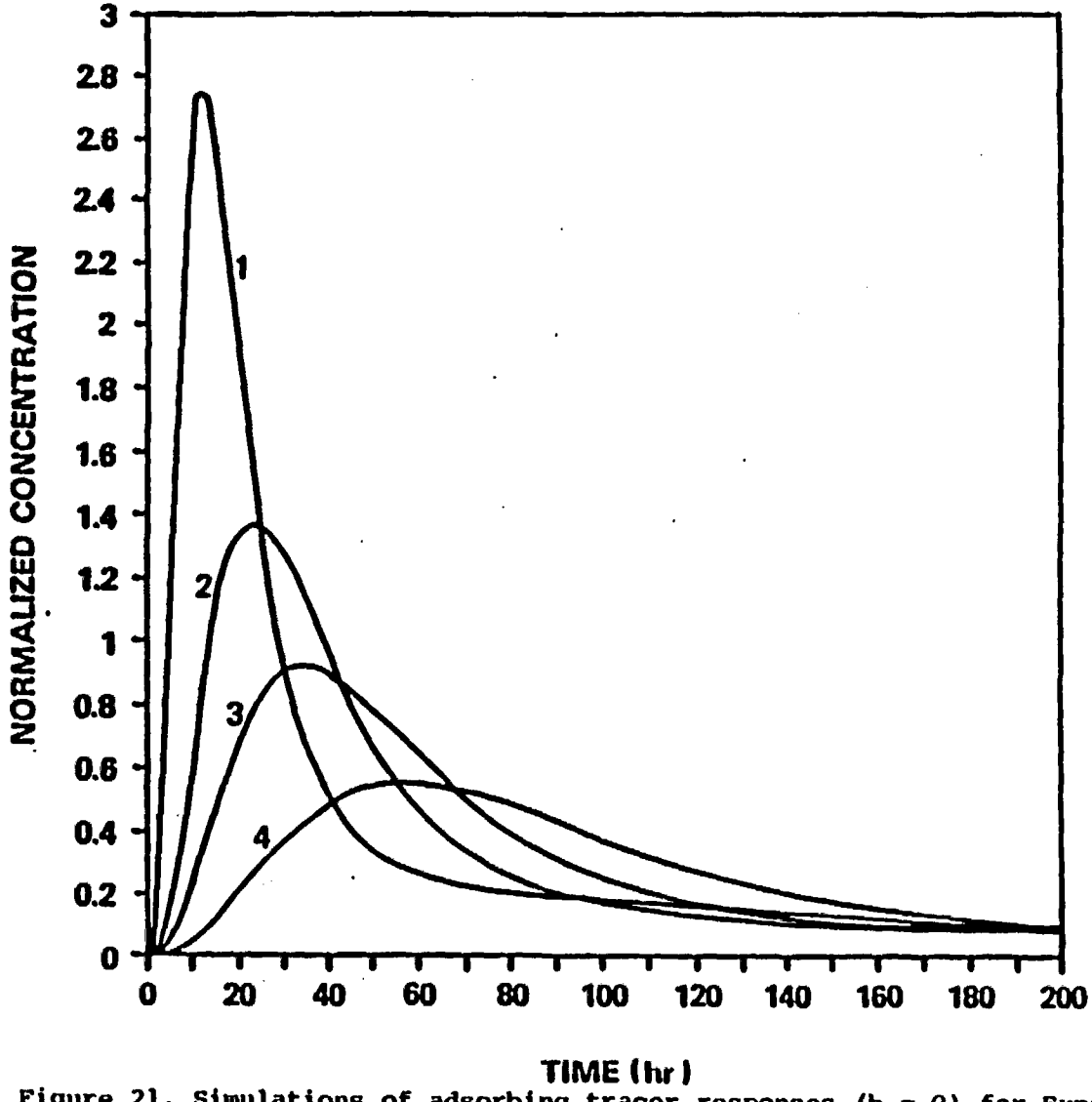

Figure 21. Simulations of adsorbing tracer responses (b = 0) for Expt. 217-A2 assuming the maximum mixedness model (1- inert tracer, 2- a_L=1, 3 - a_L=2, 4 - a_L=4).

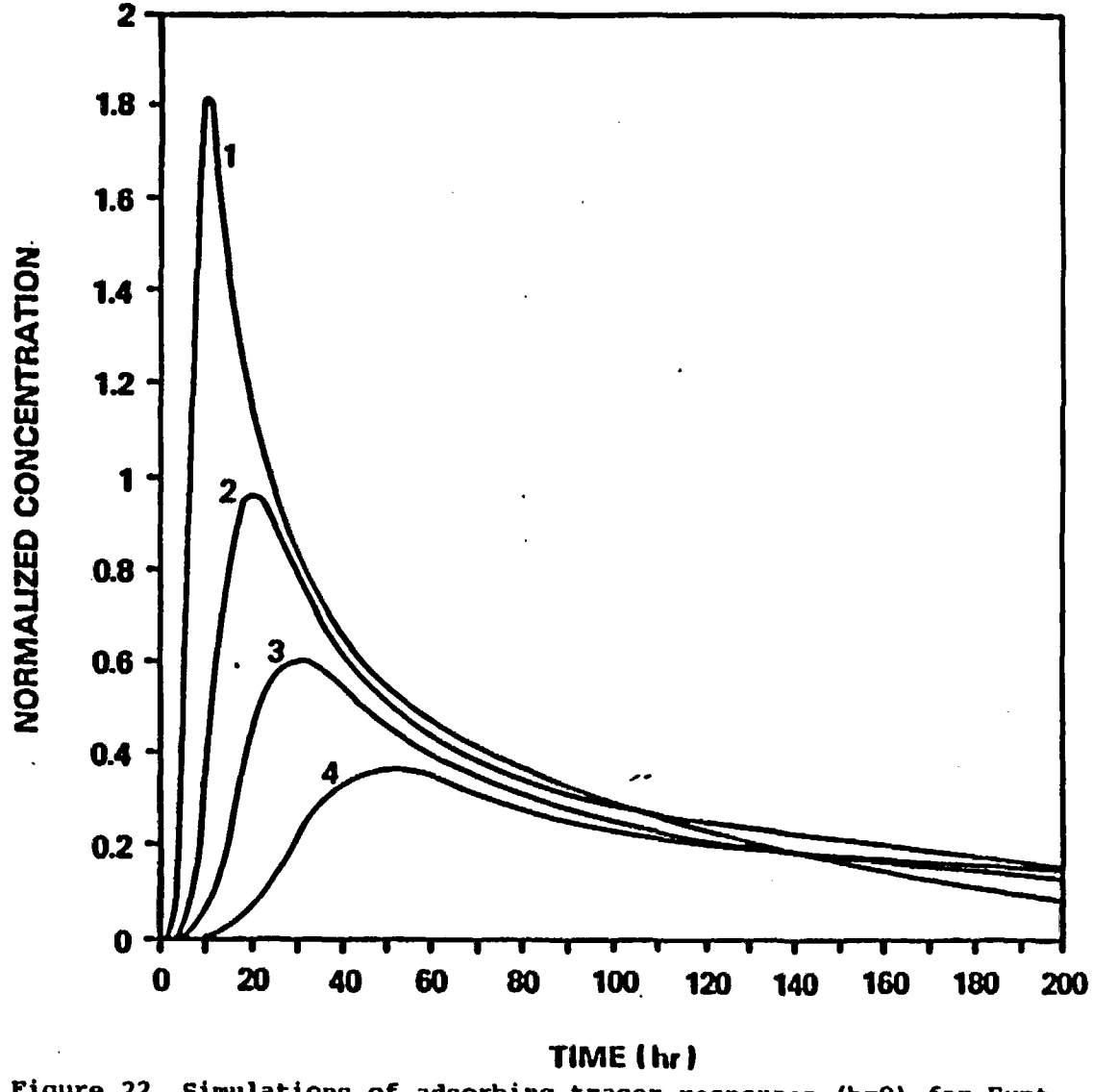

Figure 22. Simulations of adsorbing tracer responses (b=0) for Expt. 2067-T2 assuming the maximum mixedness model (1 - inert tracer, 2 - a_L=1, 3 - a_L=2, 4 - [illegible]=4).

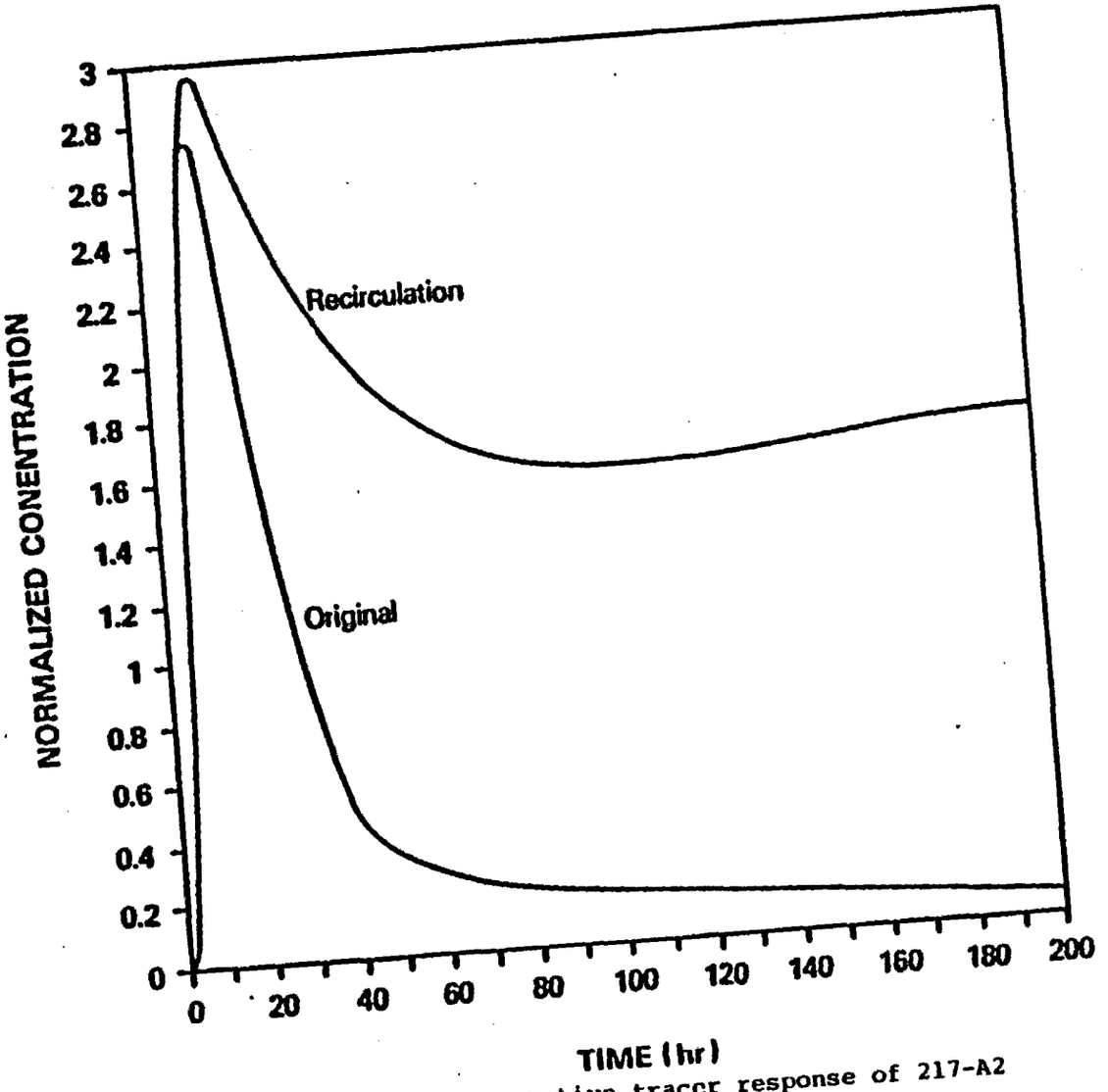

Figure 23. Simulation of conservative tracer response of 217-A2 with recirculatior

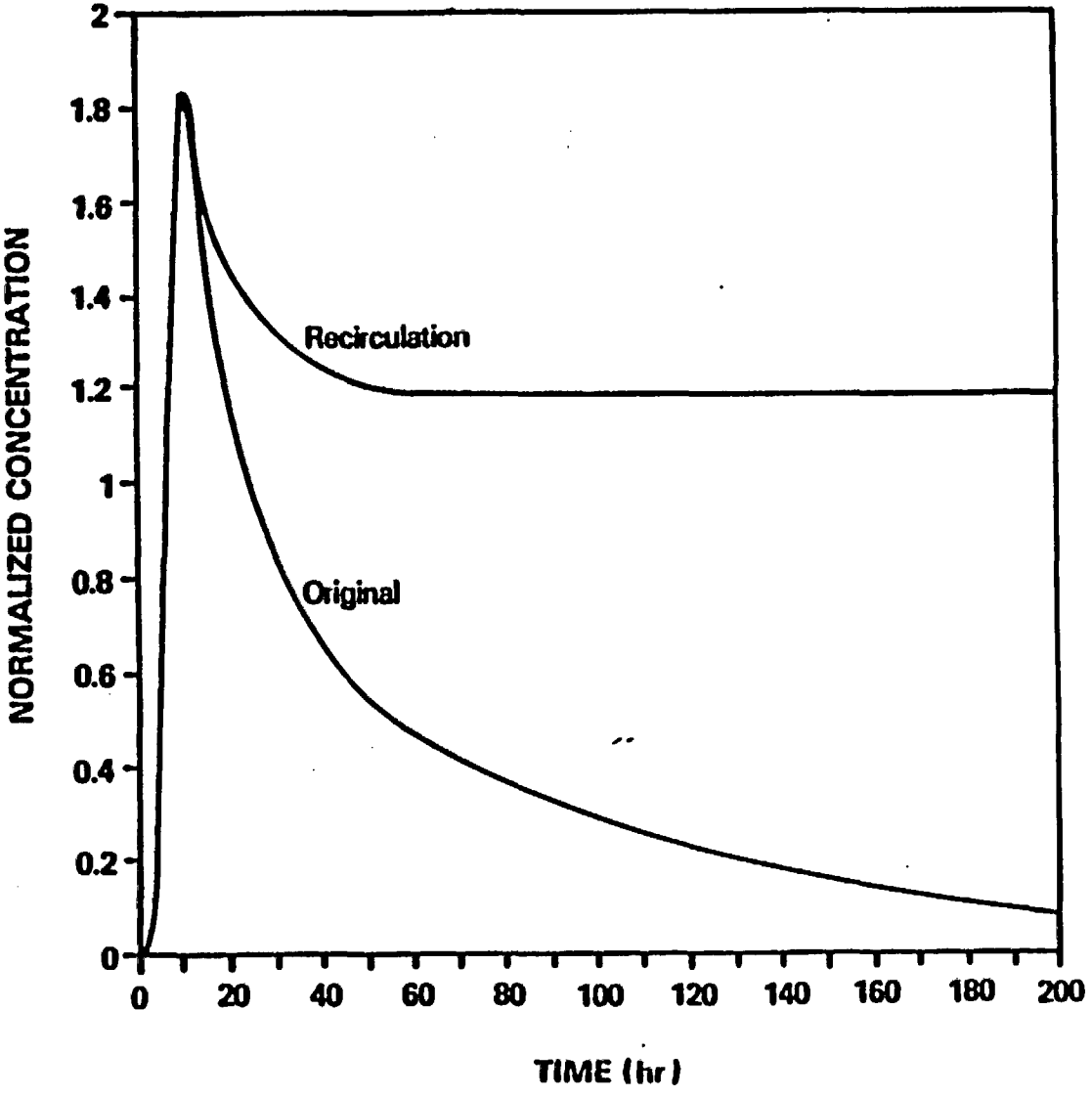

Figure 24. Simulation of a conservative tracer response of 2067-T2 with recirculation.

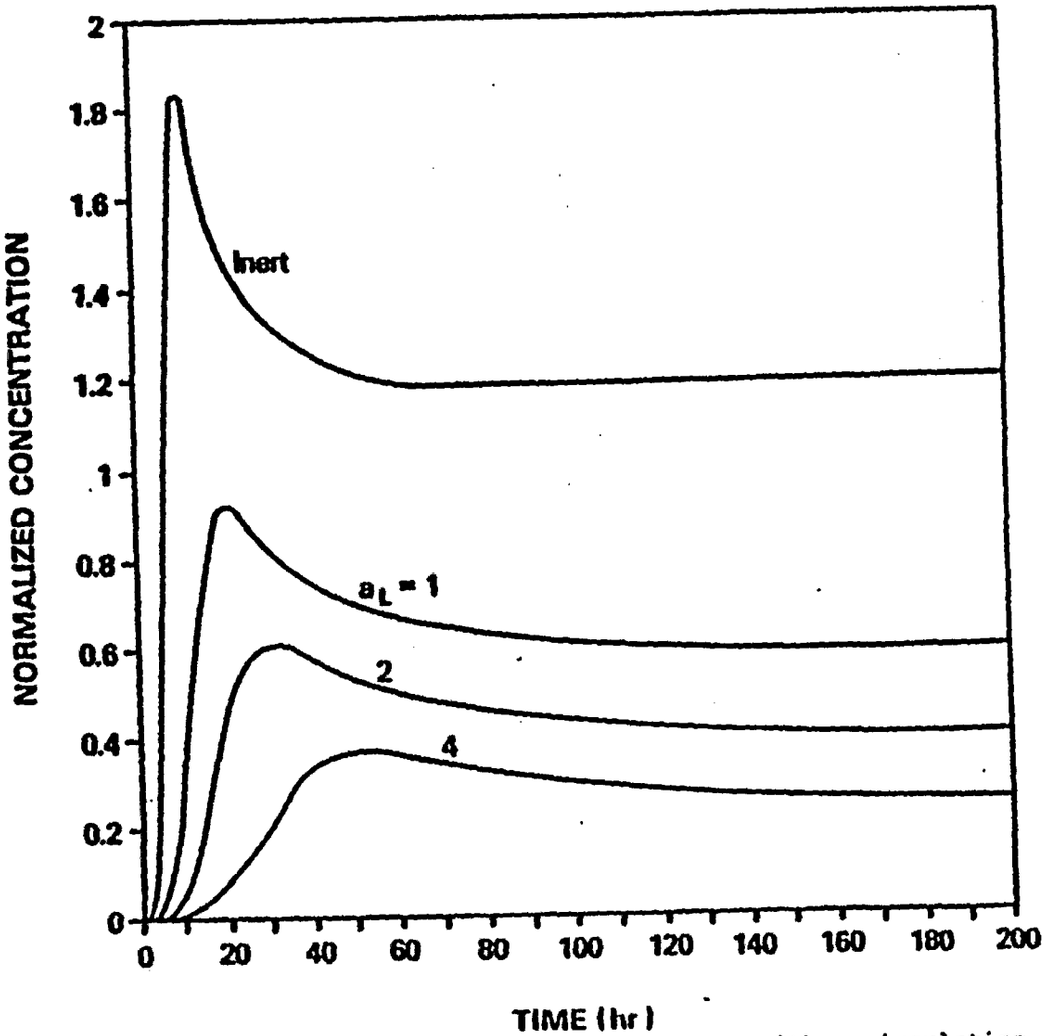

Figure 25. Simulation of sorbing tracer responses with recirculation (b=0) for 2067-T2.

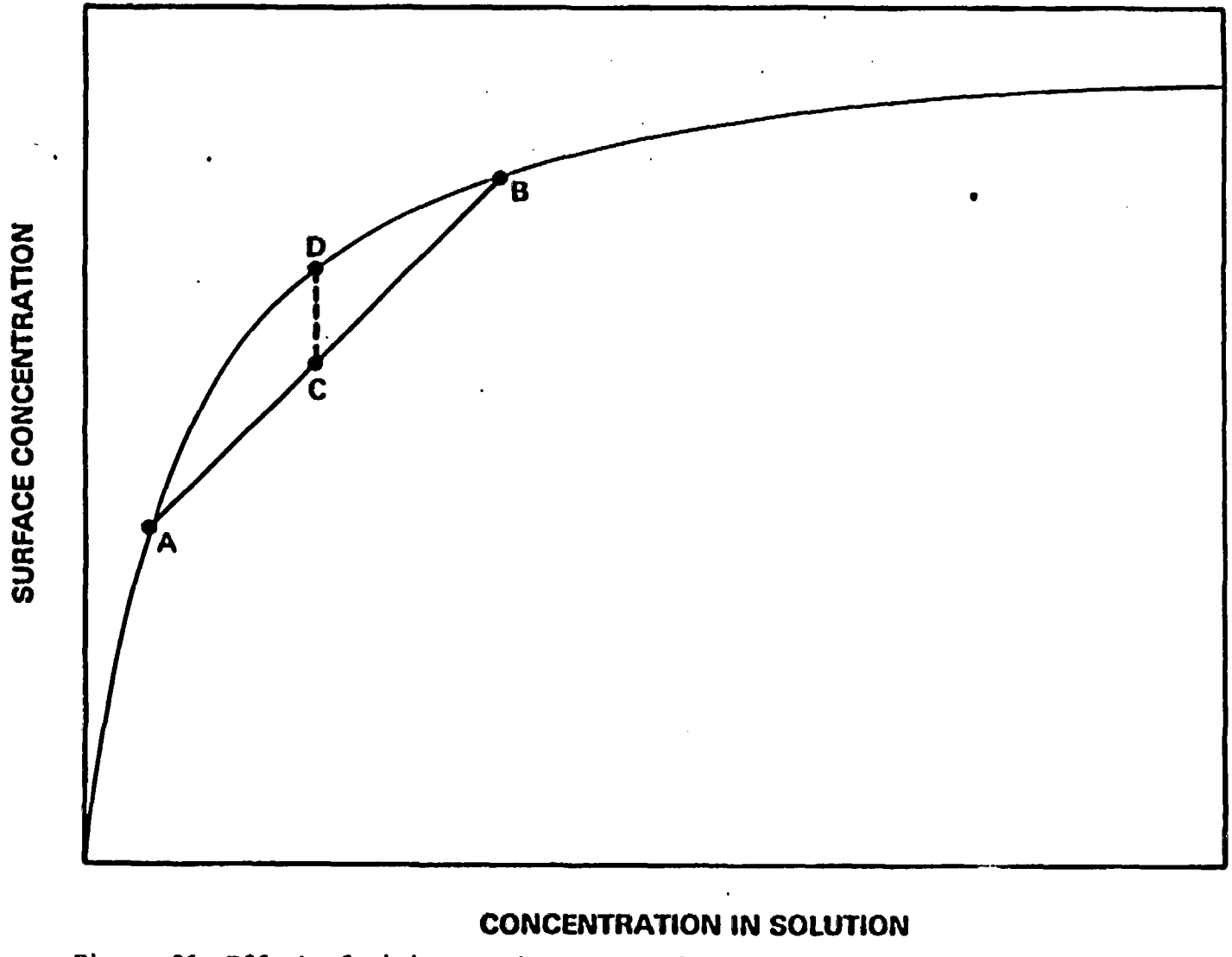

Figure 26. Effect of mixing on the amount of surface adsorption. If fluid at points A and B are mixed, sorption is denoted by D. If unmixed, sorption is denoted by C.

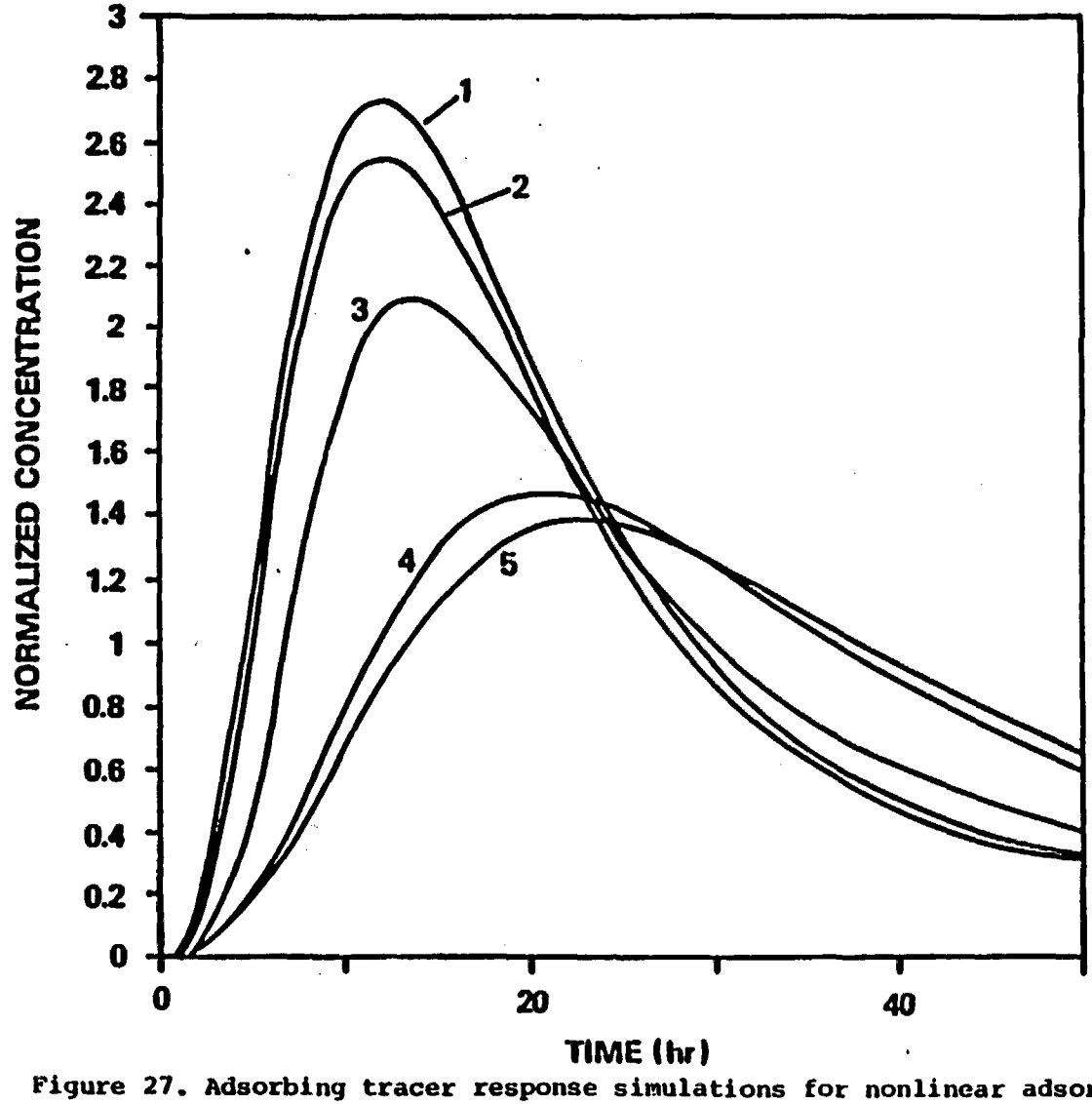

Figure 27. Adsorbing tracer response simulations for nonlinear adsorption (a_L=1, b=1) for different inlet concentrations. (1 - inert, 2 - C_{in}=1000, 3 - C_{in}) 4 - C_{in}=10, 5 - C_{in}=1).

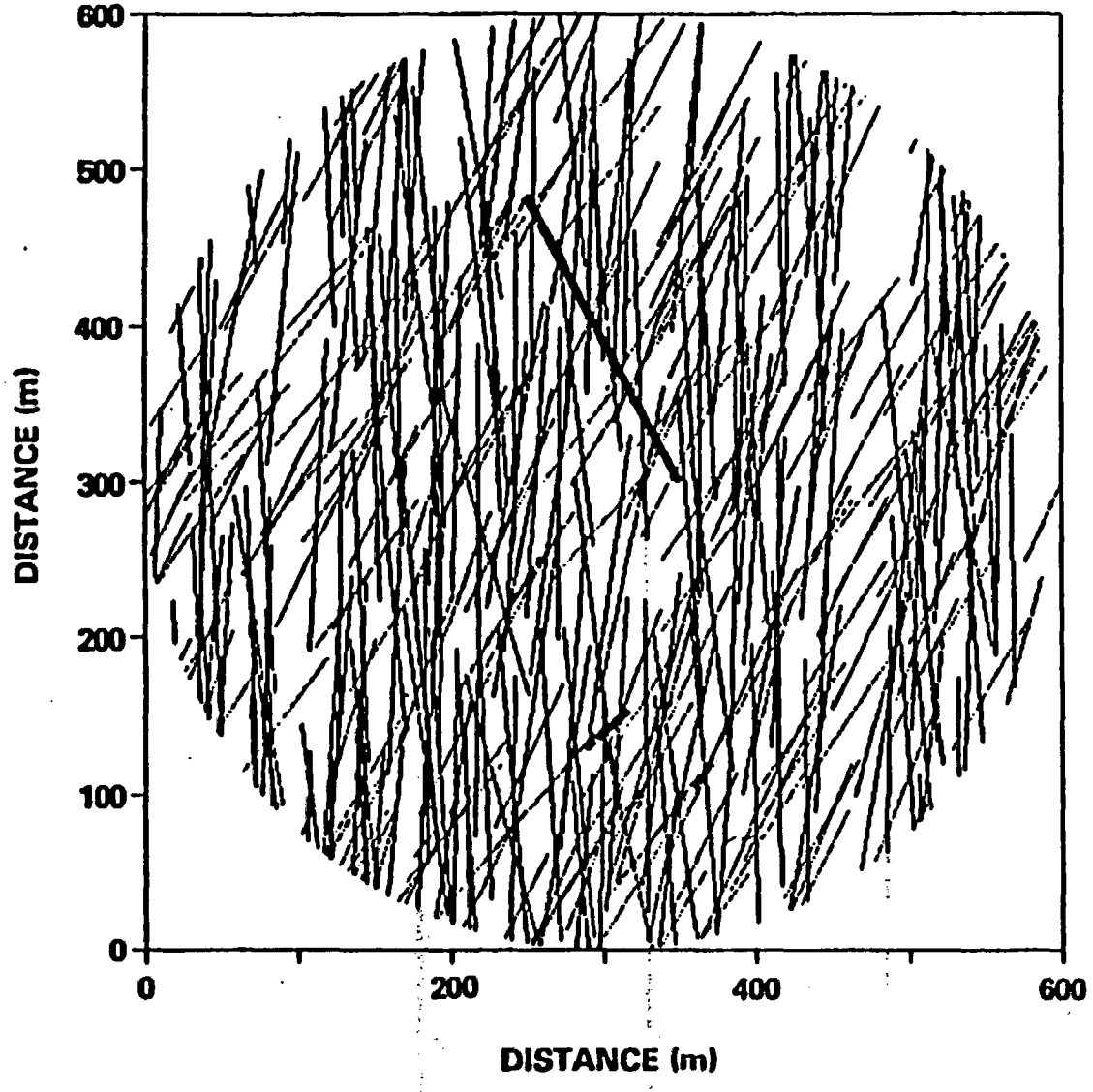

Figure 28. Fracture network and wellbore pair generated using the computer code FRACNET.

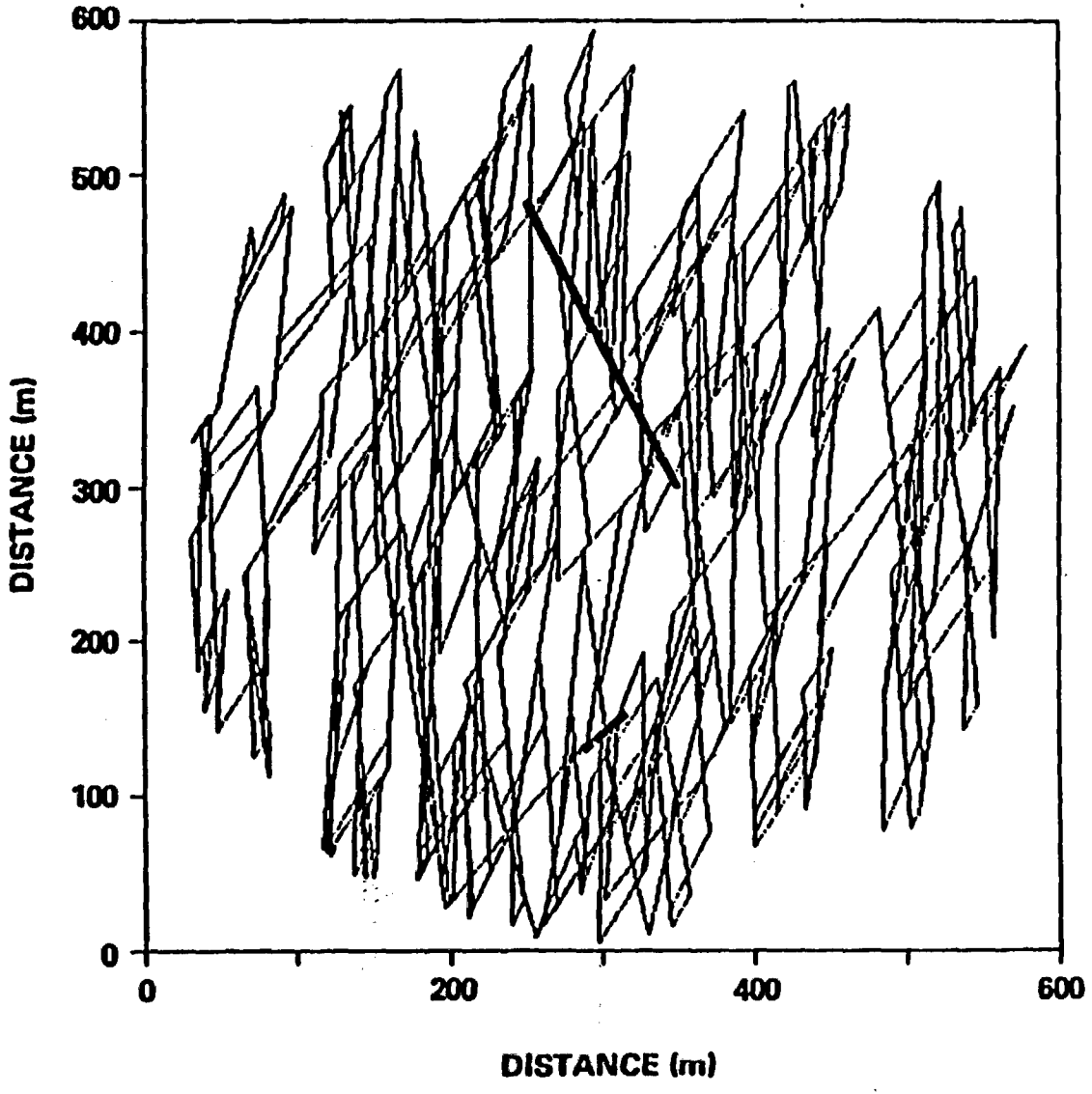

Figure 29. Connected node network for the fracture network of the previous figure.

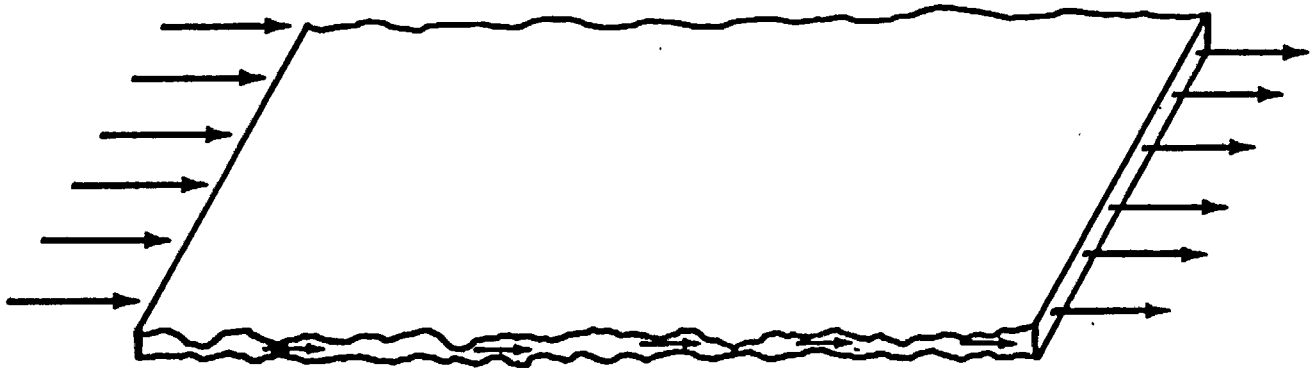

Figure 30. Schematic of flow in a rough fracture with a distribution of apertures.

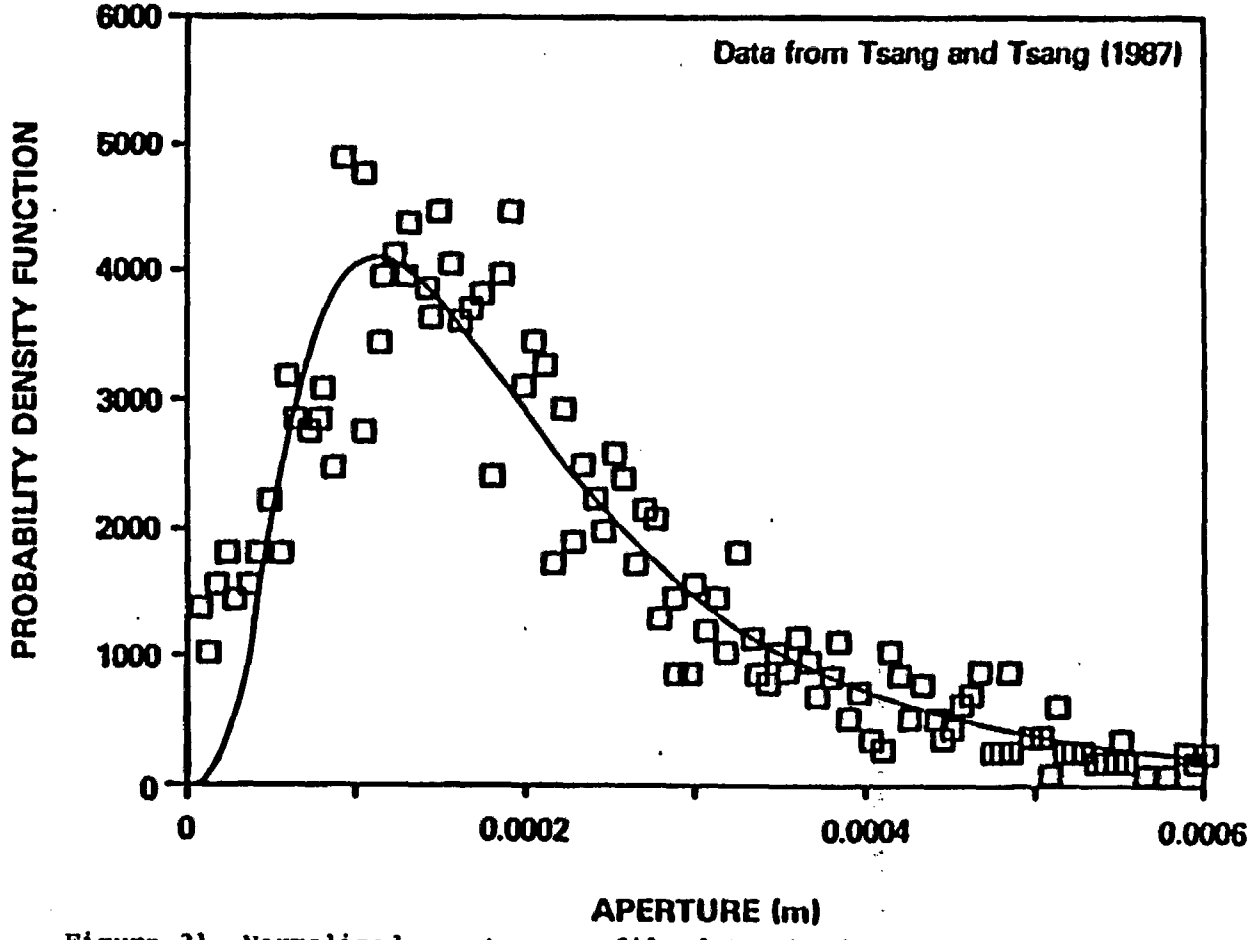

Figure 31. Normalized aperture profile data obtained by Tsang and Tsang (1987) by scanning the surfaces of a natural granite fracture in a core. The curve is the best fit to a lognormal distribution.

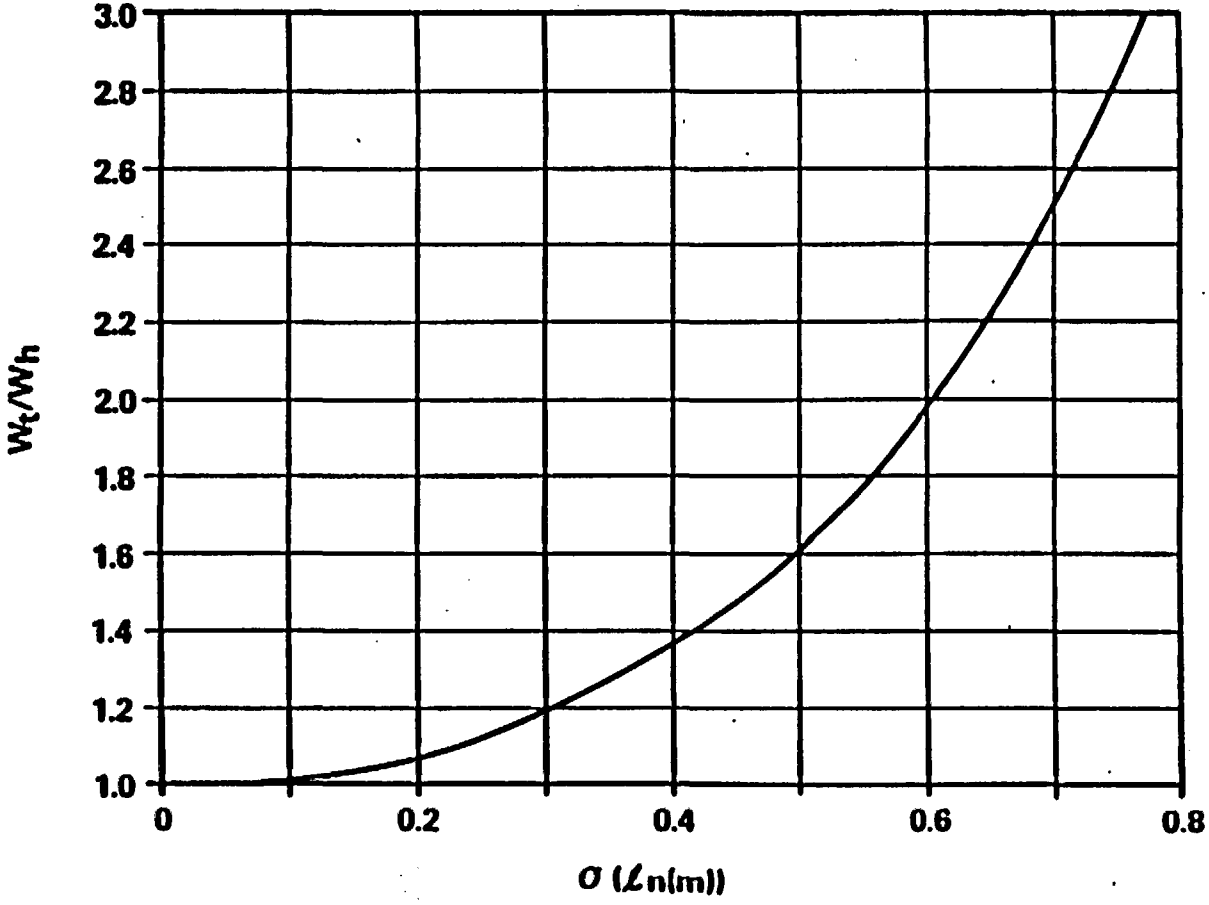

Figure 32. Calculated values of w_t/w_h versus σ for the lognormal distribution.

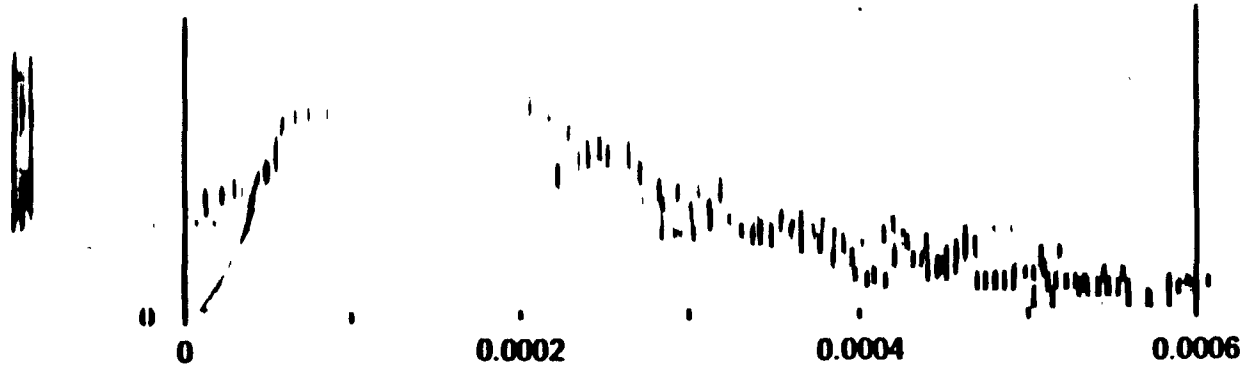

Figure 31. Normalized aperture profile data obtained by Tsang and Tsang (1987) by scanning the surface of a natural granite fracture in a core. The curve is the best fit to a lognormal distribution.

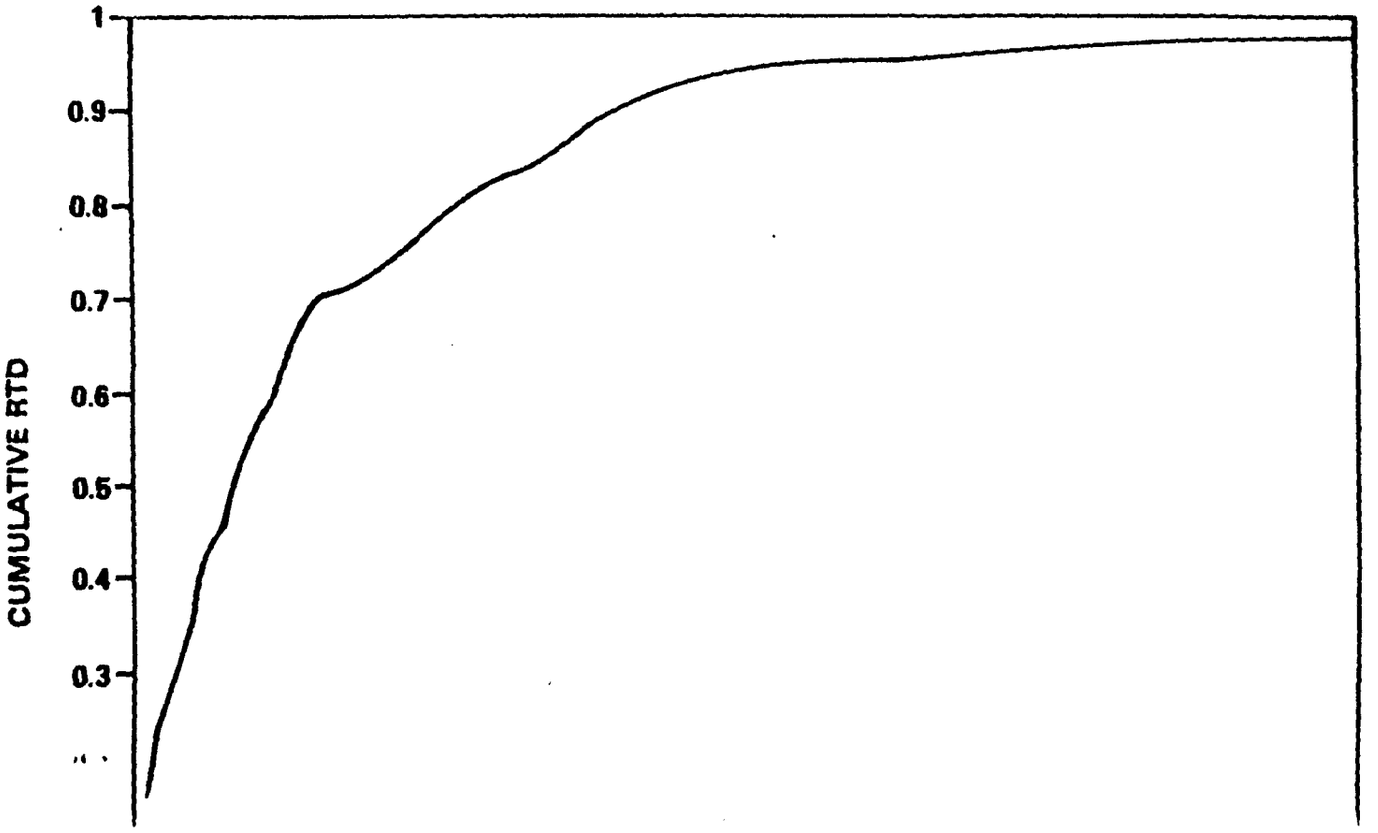
1
0.9
0.8
0.7
0.6
0.5
0.4
0.3
CUMULATIVE RTD